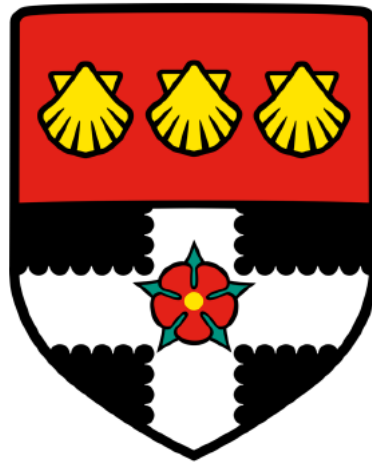


UNIVERSITY OF READING

Department of Meteorology



**Analysis of Mesoscale Convective System  
Environments over East Asia**

Xinli Ge

Supervisors: Prof. Bob Plant & Dr. Mark Muetzelfeldt

A dissertation submitted in partial fulfilment for the degree of  
Master of Science in *Applied Meteorology*.

August 2023

# Acknowledgements

Firstly, I would like to thank my supervisors, Prof. Bob Plant and Dr. Mark Muetzelfeldt, who are very nice and knowledgeable. They always give me constructive recommendations and patiently answer my questions. The encouragement they gave me allowed me to keep going. Their comments on the draft of my dissertation are very precise and helpful. Without their guidance and help, I could not complete this dissertation well.

As a weather enthusiast since 2012, yet I studied Applied Bioscience for my undergraduate degree but came here to study Applied Meteorology for my postgraduate degree. There were many difficulties along the way, but I also persevered through many cups of coffee. I would like to thank myself for being brave enough to make the decision to study Applied Meteorology here, and for persevering in the face of difficulties.

It's never too late to pursue your dreams.

# Abstract

Mesoscale convective systems (MCSs) are one of the most important weather systems affecting East Asia ( $0^{\circ}$ - $55^{\circ}$ N,  $95^{\circ}$ E- $165^{\circ}$ E). In particular, the Mei-Yu region ( $25^{\circ}$ N- $37^{\circ}$ N,  $112^{\circ}$ E- $145^{\circ}$ E) of East Asia can be affected by a large number of MCSs during the summer. East Asia has a large population density, and MCSs there can cause hazardous weather that can affect a large number of people. In the past, there have been many studies investigating MCS environments in other parts of the world, but fewer have investigated East Asia. In this study, we use a high-resolution MCS tracking database to track MCSs over East Asia and combine it with composite environmental conditions for the MCS initiation times from ERA5 to analyse the relationship between environmental conditions and MCS initiation over East Asia and the Mei-Yu region. We find that MCS initiation is most strongly associated with total column water vapour (TCWV) and moisture convergence for the East Asia region as a whole. Vertical wind shear (VWS) suppresses MCS initiation at low latitudes but promotes MCS initiation at mid-latitudes. Convective available potential energy (CAPE) has little relationship with MCS initiation. In the Mei-Yu region, TCWV, moisture convergence, and shallow VWS are the most important factors contributing to MCS initiation.

# Acronyms

|       |  |
|-------|--|
| MCSs  | Mesoscale Convective Systems                       |
| MCCs  | Mesoscale Convective Complexes                     |
| QLCSs | Quasi-Linear Convective Systems                    |
| TRMM  | Tropical Rainfall Measuring Mission                |
| SST   | Sea Surface Temperature                            |
| CAPE  | Convective Available Potential Energy              |
| LFC   | Level of Free Convection                           |
| LNB   | Level of Neutral Buoyancy                          |
| CCEWs | Convectively Coupled Equatorial Waves              |
| MJO   | Madden-Julian Oscillation                          |
| ENSO  | El Niño-Southern Oscillation                       |
| QBWO  | Quasi-BiWeekly Oscillation                         |
| ECMWF | European Centre for Medium-Range Weather Forecasts |
| ERA5  | ECMWF Reanalysis v5                                |
| JJA   | June, July and August                              |
| TCWV  | Total Column Water Vapour                          |
| VWS   | Vertical Wind Shear                                |
| VIMFD | Vertically Integrated Moisture Flux Divergence     |

# List of figures

**Figure 2-1** A radar image of a squall line with convective and stratiform precipitation components on 13 July 2015..... 4

**Figure 2-2** Schematic representation of a tropical mesoscale convective system (MCS) at mature phase. .... 5

**Figure 2-3** Contribution of MCSs to precipitation. .... 6

**Figure 2-4** Schematic representation of the effect of vertical wind shear on MCSs..... 9

**Figure 2-5** Geographic distribution and differences in the fraction of MCSs as a proportion of precipitation systems for El Niño event years and La Niña event years for the period 1998-2013. .... 11

**Figure 2-6** Schematic of the causes of the extreme Mei-Yu in the summer of 2020. .... 13

**Figure 4-1** Time series of MCS generation in East Asia from 2001 to 2020. .... 19

**Figure 4-2** Monthly MCS generation in East Asia in 2008 and 2015. .... 20

**Figure 4-3** Heat maps of MCS numbers and differences in numbers in East Asia. .... 21

**Figure 4-4** Distribution of CAPE and TCWV at the times of MCS initiation over East Asia in JJA in 2008 and 2015 and differences between the two years. .... 24

**Figure 4-5** Heat map differences in the number of MCSs between 2008 and 2015 with contours of the CAPE and TCWV differences over East Asia for both years. .... 25

**Figure 4-6** Distribution of VWS difference and VIMFD difference at the times of MCS initiation over East Asia in JJA between 2008 and 2015. .... 28

**Figure 4-7** Heat map differences of MCS number between 2008 and 2015 with contours of the VWS and VIMFD differences at the times of MCS initiation. .... 30

**Figure 4-8** Differences of environmental conditions at the times of MCS initiation in July between 2008 and 2015 (2008 -2015). .... 32

**Figure 4-9** Correlation matrix of the number of MCSs and various environmental conditions over East Asia. .... 33

|  |    |
|--|----|
| <b>Figure 4-10</b> Correlation matrix of the number of MCSs and various environmental conditions in two different regions of East Asia.....  | 35 |
| <b>Figure 4-11</b> Time series of MCS generation over the Mei-Yu region from 2001 to 2020.....   | 38 |
| <b>Figure 4-12</b> Monthly MCS generation in the Mei-Yu region in 2004 and 2020.....   | 39 |
| <b>Figure 4-13</b> Heat map differences of MCS numbers over the Mei-Yu region.....   | 40 |
| <b>Figure 4-14</b> Distribution of CAPE and TCWV at the times of MCS initiation over the Mei-Yu region in 2004 and 2020 and differences between the two years. ....  | 42 |
| <b>Figure 4-15</b> Heat map differences of MCS number between 2004 and 2020 with contours of the CAPE and TCWV differences at the times of MCS initiation over the Mei-Yu region for both years. ....        | 43 |
| <b>Figure 4-16</b> Distribution of VWS difference and VIMFD difference at the times of MCS initiation over the Mei-Yu region in JJA between 2004 and 2020.....   | 44 |
| <b>Figure 4-17</b> Heat map differences in the number of MCSs between 2004 and 2020 with contours of the VWS and VIMFD differences at the times of MCS initiation over the Mei-Yu region for both years..... | 46 |
| <b>Figure 4-18</b> Differences of MCS-initiation composite environmental conditions in July between 2004 and 2020 (2020 -2004). ....   | 47 |
| <b>Figure 4-19</b> Correlation matrix of the number of MCSs and various environmental conditions over the Mei-Yu region. ....  | 48 |

# Table of Contents

|  |            |
|--|------------|
| <b>Acknowledgements .....</b>                                  | <b>I</b>   |
| <b>Abstract.....</b>   | <b>II</b>  |
| <b>Acronyms .....</b>  | <b>III</b> |
| <b>List of figures.....</b>                                    | <b>IV</b>  |
| <br>   |            |
| <b>1 Introduction .....</b>                                    | <b>1</b>   |
| <i>1.1 Motivation.....</i>                                     | <i>1</i>   |
| <i>1.2 Objectives .....</i>                                    | <i>2</i>   |
| <b>2 Literature review.....</b>                                | <b>4</b>   |
| <i>2.1 Introduction to MCSs.....</i>                           | <i>4</i>   |
| <i>2.2 MCS initiation and environmental conditions.....</i>    | <i>7</i>   |
| <i>2.3 MCSs and large-scale drivers .....</i>                  | <i>10</i>  |
| <i>2.4 MCSs in East Asia .....</i>                             | <i>12</i>  |
| <b>3 Methodology .....</b>                                     | <b>15</b>  |
| <i>3.1 Dataset.....</i>  | <i>15</i>  |
| <i>3.2 Methods of analysing environmental conditions .....</i> | <i>16</i>  |
| <i>3.3 Methods of statistical analysis.....</i>                | <i>17</i>  |
| <b>4 Results .....</b>   | <b>18</b>  |
| <i>4.1 Analysis of MCS environments over East Asia.....</i>    | <i>18</i>  |
| 4.1.1 Time series of MCS number .....                          | 18         |
| 4.1.2 Comparison between 2008 and 2015 .....                   | 20         |
| 4.1.3 Analysis of thermodynamic conditions.....                | 23         |
| 4.1.4 Analysis of dynamic conditions.....                      | 27         |
| 4.1.5 Analysis of individual months .....                      | 32         |
| 4.1.6 Correlation analysis .....                               | 33         |

|  |           |
|--|-----------|
| <i>4.2 Analysis of MCS environments over the Mei-Yu region</i> ..... | 36        |
| 4.2.1 Time series of MCS number .....                                | 37        |
| 4.2.2 Comparison between 2004 and 2020 .....                         | 39        |
| 4.2.3 Analysis of thermodynamic conditions.....                      | 41        |
| 4.2.4 Analysis of dynamic conditions .....                           | 43        |
| 4.2.5 Analysis of individual months .....                            | 46        |
| 4.2.6 Correlation analysis .....                                     | 48        |
| <b>5 Discussion</b> .....  | <b>50</b> |
| 5.1 MCS inter-annual and inter-monthly comparisons .....             | 50        |
| 5.2 MCS environments over East Asia .....                            | 51        |
| 5.3 MCS environments over the Mei-Yu region.....                     | 53        |
| 5.4 Limitations and future work .....                                | 54        |
| <b>6 Conclusion</b> .....  | <b>55</b> |
| <b>References</b> .....  | <b>57</b> |

# 1 Introduction

## 1.1 Motivation

Mesoscale convective systems (MCSs) are weather systems that are hundreds of kilometres long and last for hours or even days (Houze 2004). The initiation of MCSs is affected by many environmental conditions. The three essential ingredients for MCS initiation are moisture, lift and instability (Johns and Doswell 1992; Schultz et al. 2000). Moisture and instability can be measured in convective available potential energy (CAPE, Schultz et al. 2000). In addition to this, MCS initiation is also affected by total column water vapour (TCWV, Chen et al. 2017), moisture convergence (Raymond and Fuchs-Stone 2021; Tomassini 2021) and vertical wind shear (VWS, Grant et al. 2020; Coniglio and Stensrud 2001).

The activity of MCSs has a strong bearing on human life. Precipitation from MCSs can account for 50%-90% of the total annual precipitation at low and middle latitudes (Nesbitt et al. 2006). MCSs provide moisture to the soil and bring the precipitation necessary for agriculture; too few MCSs can cause droughts (Schumacher and Rasmussen 2020), and too many can cause extreme weather such as floodings and mudslides (Rasmussen and Houze 2012). Currently, there have been several studies that have investigated changes in the number of MCSs in some parts of the globe, as well as changes in environmental conditions. Since 1982, the number of intense MCSs in the West African Sahel has continued to increase, which is associated with increased warming of the Sahara driven by anthropogenic forcing (Taylor et al. 2017). The intensity of MCSs in the central U.S. is increasing in the spring, which is closely related to strengthening of the low-level jet (Feng et al. 2016).

East Asia ( $0^{\circ}$ - $55^{\circ}$ N,  $95^{\circ}$ E- $165^{\circ}$ E) is one of the most important regions affected by MCSs, with large population densities (Schumacher and Rasmussen 2020). In June, a quasi-stationary front called the Mei-Yu front occurs in parts of East Asia ( $25^{\circ}$ N - $37^{\circ}$ N,  $112^{\circ}$ E- $145^{\circ}$ E), associated with which many MCSs are produced and much precipitation is caused (Zhang et al. 2018). In the summer of 2020, record-breaking Mei-Yu fronts with long-lasting, wide

meridional rainbands and intense precipitation brought severe flooding to East Asia (Ding et al. 2021). Due to the lack of high temporal and spatial resolution observations, MCSs in East Asia have been less studied in the past compared to other regions (Li et al. 2020). Therefore, it is necessary to investigate the environmental conditions for MCS initiation over East Asia.

This study uses a high-resolution MCS tracking database (Feng et al. 2021) to track MCSs over East Asia, combined with ERA5 (Hersbach et al. 2020) data on MCS initiation to construct composite environmental conditions to investigate the environmental conditions for MCS initiation.

## **1.2 Objectives**

At present, research on MCSs in East Asia is more often based on the analysis of specific cases of MCS development (Li et al. 2020), with relatively fewer investigations of the environmental conditions for MCS initiation. Hence, there is an urgent necessity to analyse the environmental conditions for MCS initiation over East Asia.

The main objectives of this study are to investigate whether the frequency of MCSs has changed over the past two decades over East Asia and the Mei-Yu region, to investigate the effects of different MCS initiation composite environmental conditions on MCS initiation. We will focus on which environmental conditions have the greatest effect on MCS initiation, and further investigate whether the effects of environmental conditions on MCS initiation vary over different latitudinal ranges over East Asia.

This study is organized as follows: Section 2 provides a literature review of the basic properties, initiation, environmental conditions, and relationship with large-scale drivers of MCSs, and describes the existing literature on MCSs in East Asia; Section 3 describes the datasets and analysis methods used in this study; Section 4 presents the results of the investigation of the environmental conditions for MCS initiation in East Asia and the Mei-Yu region as well as some interpretations of the results; Section 5 discusses the MCS initiation

composite environmental conditions investigated in this study with the context of the existing literature; and finally a summary and conclusions on the MCS environments over East Asia are given in Section 6.

## 2 Literature review

### 2.1 Introduction to MCSs

Convection and precipitation are among the major meteorological phenomena in the atmosphere. They are caused mainly by small- and mesoscale weather systems under the influence of large-scale conditions. Organised convective cloud masses that are hundreds or even thousands of kilometres long on spatial scales and last for hours or even more than a day on time scales are defined as mesoscale convective systems (MCSs, Houze, 2018). One of the special cases of MCSs is mesoscale convective complexes (MCCs), which are characterised by being huge, long-lasting and quasi-circular (Maddox 1980). MCSs that show up as long, bow-shaped echoes on radar images are referred to squall lines or quasi-linear convective systems (QLCSs, Weisman and Davis 1998).

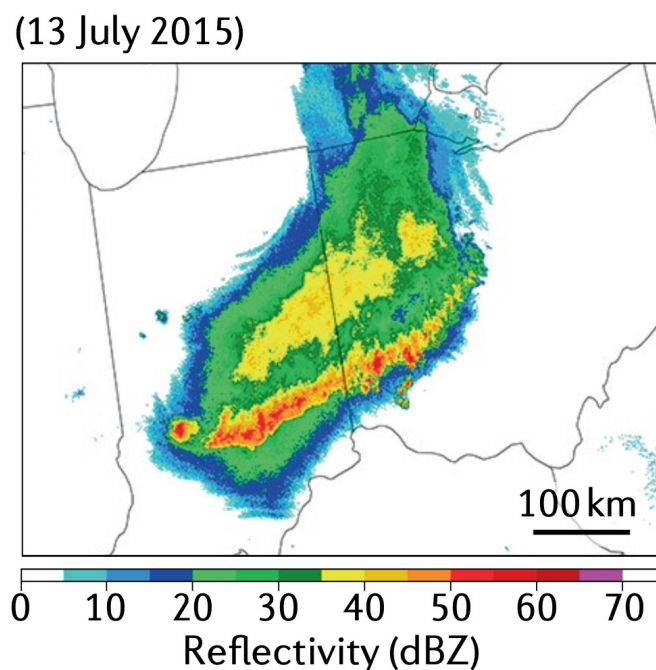


**Figure 2-1** A radar image of a squall line with convective and stratiform precipitation components on 13 July 2015. From Schumacher and Rasmussen (2020).

MCSs have both convective and stratiform precipitation components (Figure 2-1, Houze, 2004). The stratiform precipitation results from a combination of the dissipation of mature convective cells and the extensively sloped ascent of mesoscale layers (Houze et al. 1989). Figure 2-2 shows the structure of an MCS at a mature phase, where the presence of both convective and stratiform precipitation regions is a characteristic of an MCS at a mature phase (Houze 2018).

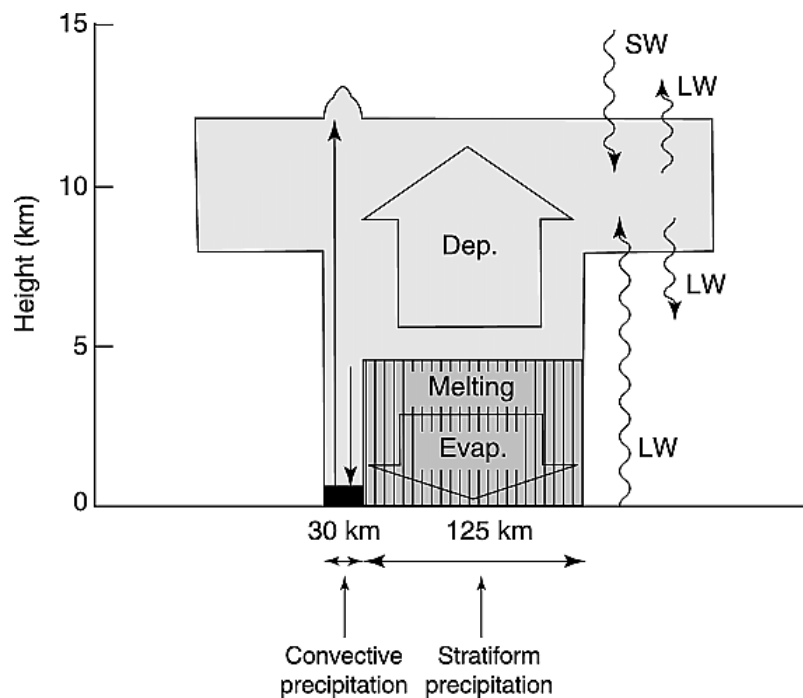


**Figure 2-2** Schematic representation of a tropical mesoscale convective system (MCS) at mature phase. LW represents long-wave radiation, and SW represents short-wave radiation. Light shading, light shading with vertical lines and black shading indicates cloud coverage, stratiform precipitation areas and convective precipitation areas, respectively. Wide, open arrows illustrate mesoscale ascent and subsidence in the stratiform regions, while straight, solid arrows illustrate convective updrafts and downdrafts. From Houze (2004).

Just as there are diurnal and seasonal cycles for solar energy, MCSs also exhibit significant temporal variability (Schumacher and Rasmussen 2020). Here, we consider US studies as an example. In the United States, MCSs occur mostly during the warmer months of May through August, mainly due to abundant water vapour and instability (Haberlie and Ashley 2019). As

for the diurnal cycle, over land, due to the increased instability of the land surface, MCSs are generally initiated in the afternoon or early evening (Nesbitt and Zipser 2003). Geerts et al. (2017) suggested that precipitation during the warm season in the central Great Plains region of North America reached a maximum at night, with most of the precipitation being from MCSs. In addition to instability, another important reason for this diurnal cycle in the US is that the Great Plains low-level jet also play a very important role in this process (Higgins et al. 1997). MCSs dissipate within a few hours after sunrise (Laing and Michael Fritsch 1997). Such diurnal and seasonal cycles also apply to Europe (Morel and Senesi 2002).

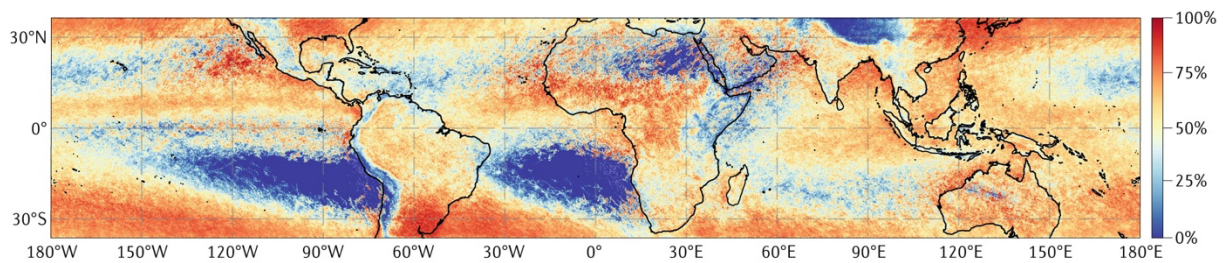


**Figure 2-3** Contribution of MCSs to precipitation. The data for these three figures are based on observations from the Tropical Rainfall Measuring Mission (TRMM) satellite from December 1997 to September 2014 between 36°S and 36°N. From Schumacher and Rasmussen (2020).

MCSs are involved in the tropical and subtropical hydrologic cycle and occupy a very important position. As shown in Figure 2-3, the Tropical Rainfall Measuring Mission (TRMM, Kummerow et al. 1998; Simpson et al. 1988) observations show that MCSs contribute 50%-90% of annual precipitation to tropical and subtropical regions (Nesbitt et al. 2006). MCSs, particularly those that are slow-moving and long-lasting, are often associated with hazardous weather, bringing strong winds, heavy rain, hail and even tornadoes (Johns and Hirt 1987). In the United States, more than half of the 100-yr, 24-h extreme precipitation events are caused by MCSs (Stevenson and Schumacher 2014). MCSs play a significant role in causing slow-rising and hybrid flooding throughout the warm season in the central United States (Hu et al. 2021). In some regions, MCSs have caused very serious disasters, for example, floods and mudslides in Pakistan in 2010 (Rasmussen and Houze 2012). On the other hand, MCSs bring necessary

water resources for agricultural production to tropical and subtropical regions. Therefore, if the frequency of MCSs decreases, it may bring drought to agriculturally productive areas such as the Great Plains of the US and much of Asia (Schumacher and Rasmussen 2020).

In the context of global warming, the hydrological cycle is expected to intensify, with extreme precipitation occurring more frequently, resulting in more flooding and posing serious hazards to society (Allen and Ingram 2002). As a major source of precipitation in the tropics and subtropics (Figure 2-3), the frequency of MCSs has also increased in some regions. Prein et al. (2017) used a North American-scale convection-permitting model to show that the number of MCSs occurring in the summer will more than triple in North America. Taylor et al. (2017) found that the frequency of Sahelian storms has doubled since 1982. Kahraman et al. (2021) used climate simulations to show that the MCSs in Europe will become slower moving, resulting in longer durations of heavy precipitation, thus making floods more frequent in Europe. Therefore, changes in the properties of MCSs in the context of climate change pose a very serious challenge for mankind. Hence, the study of the environmental conditions that cause changes in the frequency of the generation of MCSs becomes a topic of great significance.

## **2.2 MCS initiation and environmental conditions**

At present, there are still limitations in the studies of the mechanisms involved in the initiation and upscale growth of convection in MCSs (Galarneau et al. 2023). There are two main theories of the interaction between convection and atmospheric circulation (Tomassini 2021). One theory is that the initiation of convection is largely controlled by low-level atmospheric circulation conditions through the associated changes in moisture convergence and convective inhibition (Charney and Eliassen 1964). In this theory, low-level inhibition and the conditional instability of the atmosphere allow convection to drive and enhance synoptic-scale disturbances and overturning circulations through vertical motion and latent heating (Tomassini 2021). Another theory is the convective quasi-equilibrium theory, which views convection as a process of adjustment in response to larger-scale instabilities (Emanuel et al. 1994). Since low-

level inhibition is not considered as a dominant controlling barrier, it is believed that convection effectively balances and mitigates vertical instabilities at a rate commensurate with their generation by larger-scale processes throughout the vertical atmosphere (Tomassini 2021). Now, a new theory called the "lower-tropospheric quasi-equilibrium" is evolving, which recognises the influence of lower-mid tropospheric moisture on convection and the importance of moist convection in initiating and establishing circulations (Raymond and Herman 2011; Raymond et al. 2015). MCSs initiation also follows a similar pattern to the mesoscale sea surface temperature (SST) gradient zones (Li and Carbone 2012).

As for the environmental conditions for MCSs generation, the ingredients-based methodology states that three ingredients are required for the occurrence of deep, moist convection: moisture, lift and instability (Johns and Doswell 1992; Schultz et al. 2000). To be specific, moisture is needed to get sufficient water vapour to condense and form precipitation, lift is needed to drive the formation of instability, and instability is needed to give the air a constant upward acceleration (Schumacher and Rasmussen 2020). The magnitude of these ingredients can be expressed in terms of convective available potential energy (CAPE), which is obtained by integrating the buoyancy with height from the level of free convection (LFC) up to the level of neutral buoyancy (LNB, Schultz et al. 2000). The formula for CAPE can be expressed as Equation 2-1:

$$CAPE = \int_{p_{LNB}}^{p_{LFC}} R_d(T_p - T_a) d \ln p \quad (2 - 1)$$

where  $p_{LFC}$  is the pressure of LFC,  $p_{LNB}$  is the pressure of LNB,  $R_d$  is specific gas constant for dry air,  $T_p$  is the temperature of the air parcel,  $T_a$  is the temperature of the air in environment,  $p$  is the pressure. Convection only develops when these ingredients are in place (Schumacher and Rasmussen 2020).

Currently, there have been many studies investigating the significant role of moisture in the development of moist convection (Bretherton et al. 2004; Sherwood et al. 2004). Total column water vapour is the most dominant single factor in the formation of a precipitation system (Chen et al. 2017). The probability of precipitation increases considerably with column

water vapour (Holloway and Neelin 2010). When moisture in the environment is high, MCSs will produce precipitation more efficiently (Holloway and Neelin 2009). The organization of stratiform precipitation within the linear MCSs is significantly influenced by the maximum level of water vapor transport and the storm-relative flow in its surrounding area (Parker and Johnson 2000). Raymond and Fuchs-Stone (2021) analysed the conditions of tropical ocean convection through two field projects on tropical oceans, revealing the importance of moisture convergence for MCSs initiation.

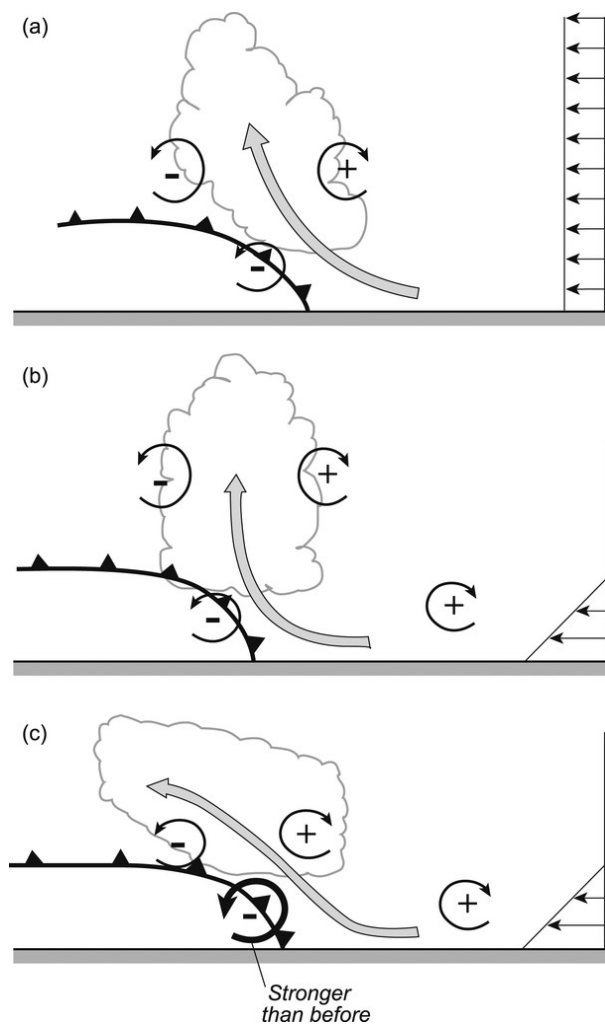


**Figure 2-4** Schematic representation of the effect of vertical wind shear on MCSs. + and - represent horizontal vorticity. (a) In the case where there is no vertical wind shear; (b) in the initial phase where vertical wind shear is present; and (c) in the mature phase where vertical wind shear is present. From Houze (2018)

Vertical wind shear, which is a change in wind direction and speed in the vertical direction, is also a required ingredient if convective storms are to develop into larger structures (Schumacher and Rasmussen 2020). Figure 2-4 shows the effect of vertical wind shear on the intensity of MCSs, which contributes to the intensification of MCSs (Houze 2018). There have been a number of simulations demonstrating the important role of vertical wind shear in the development of MCSs (Grant et al. 2020; Coniglio and Stensrud 2001). Chen et al. (2015) investigated the effect of different levels of vertical wind shear on the development of MCSs: an increase in low-level wind shear has a positive effect on the production of more organised quasi-linear convective systems, an increase in mid-level wind shear has a strong effect on the increase in vorticity and thus tends to produce supercells of isolated, strong storms, and upper-level wind shear reduces convective strength but has little effect on the structural organisation of the convection. However, Coniglio et al. (2006) suggested through 2D experimental investigations that upper-level vertical wind shear contributes to the maintenance of convection and increases the magnitude and precipitation intensity of MCSs.

With these essential ingredients for development, MCSs are also often generated in synoptic systems such as cold fronts (Schumacher and Rasmussen 2020). For example, during the warm season in the USA, much of the generation of MCSs is associated with quasi-stationary fronts (Trier et al. 2014).

## **2.3 MCSs and large-scale drivers**

MCSs are one of the most important links between convective activity and large-scale circulations in the atmosphere and are associated with large-scale wave motion in various forms (Houze 2004).

MCSs are considered to be components of large-scale convectively coupled equatorial waves (CCEWs, Cheng et al. 2023). CCEWs can modulate tropical environments, which can contribute to convection initiation and organization (Kiladis et al. 2009). This modulation not only affects the cloud complex as a whole and changes the likelihood of MCS occurrence, but

also increases the frequency and magnitude of MCS as the CCEWs become active, producing more precipitation and a greater likelihood of extreme MCSs (Nakamura and Takayabu 2022a,b; Cheng et al. 2023). Cheng et al. (2023) suggested that these changes are most pronounced due to Kelvin waves and tropical depression-type waves, and less pronounced due the Madden-Julian Oscillation (MJO).

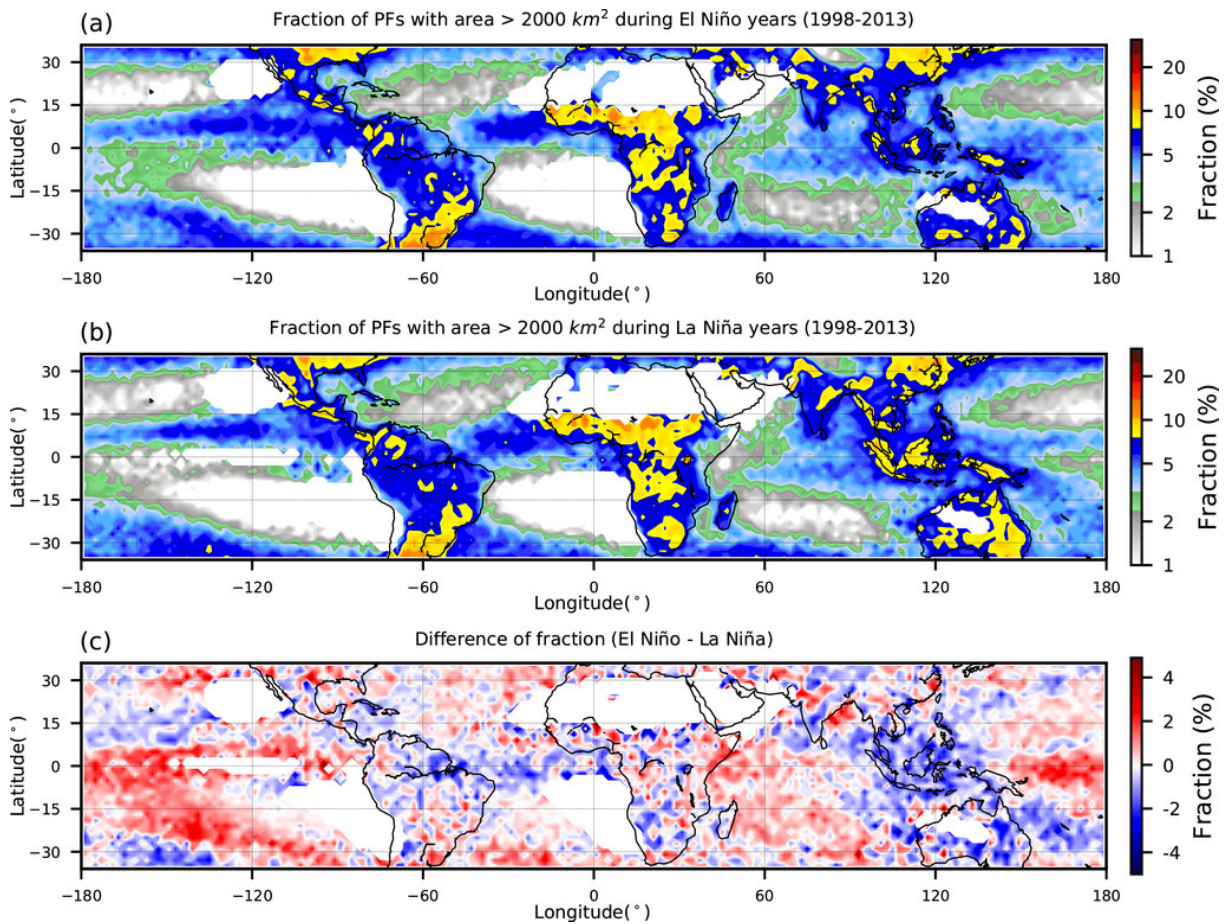


**Figure 2-5** Geographic distribution and differences in the fraction of MCSs as a proportion of precipitation systems for El Niño event years and La Niña event years for the period 1998-2013. (a) during El Niño events, (b) during La Niña events, and (c) differences between El Niño and La Niña events. From Liu et al. (2019).

It is widely recognised that El Niño-Southern Oscillation (ENSO) events have an impact on MCSs, which means that the number and distribution of MCSs will be different in years with La Niña events than in years with El Niño events (Zolman et al. 2000). Liu et al. (2019)

counted MCSs as a proportion of the total precipitation systems for El Niño and La Niña event years and counted the differences (Figure 2-5). El Niño event years have a smaller proportion of MCSs in the South China Sea and around the Philippines than La Niña event years, whereas El Niño event years have a larger proportion of MCSs in eastern China than La Niña event years (Figure 2-5 c, Liu et al. 2019). Convection in southern Africa during the summer is also strongly influenced by ENSO, that is, convective systems tend to contract towards the equator during El Niño events, while convective systems are southward-biased and intensify during La Niña events (Hart et al. 2019).

## **2.4 MCSs in East Asia**

East Asia has a large population and a high population density. East Asia is also one of the main regions affected by MCSs (Schumacher and Rasmussen 2020). However, most of the existing studies on MCSs are based on the USA or on the tropics in a broad sense, while MCSs in East Asia have been less studied in the past due to the lack of high temporal and spatial resolution observations (Li et al. 2020).

The Tibetan Plateau profoundly affects the weather in East Asia and even globally, and also has a profound impact on MCSs (Fu et al. 2019). The eastern margin of the Tibetan Plateau frequently generates long-lived MCSs (Li et al. 2020). Yang et al. (2019) analysed the eastward propagating MCSs formed from the eastern side of the Tibetan plateau and found that stronger low-level cyclonic vorticity is favourable to the maintenance of MCSs and that more moisture is favourable to prolonging the active life of MCSs. Yang et al. (2020) revealed that the favourable conditions for the formation of eastward propagating MCSs are the combination of a mid-level trough in the eastern Tibetan Plateau and the west Pacific subtropical high.

The East Asian monsoon system and the Indian monsoon system are independent of but also interact with each other, and they form a large Asian summer monsoon system (Ding and Chan 2005). In East Asia, there is a complex interaction between MCSs and the large-scale monsoon circulation (Li et al. 2020). The strength and poleward propagation of the East Asian

summer monsoon is mainly influenced by the subtropical westerly jet and the subtropical high (Volonté et al. 2022).

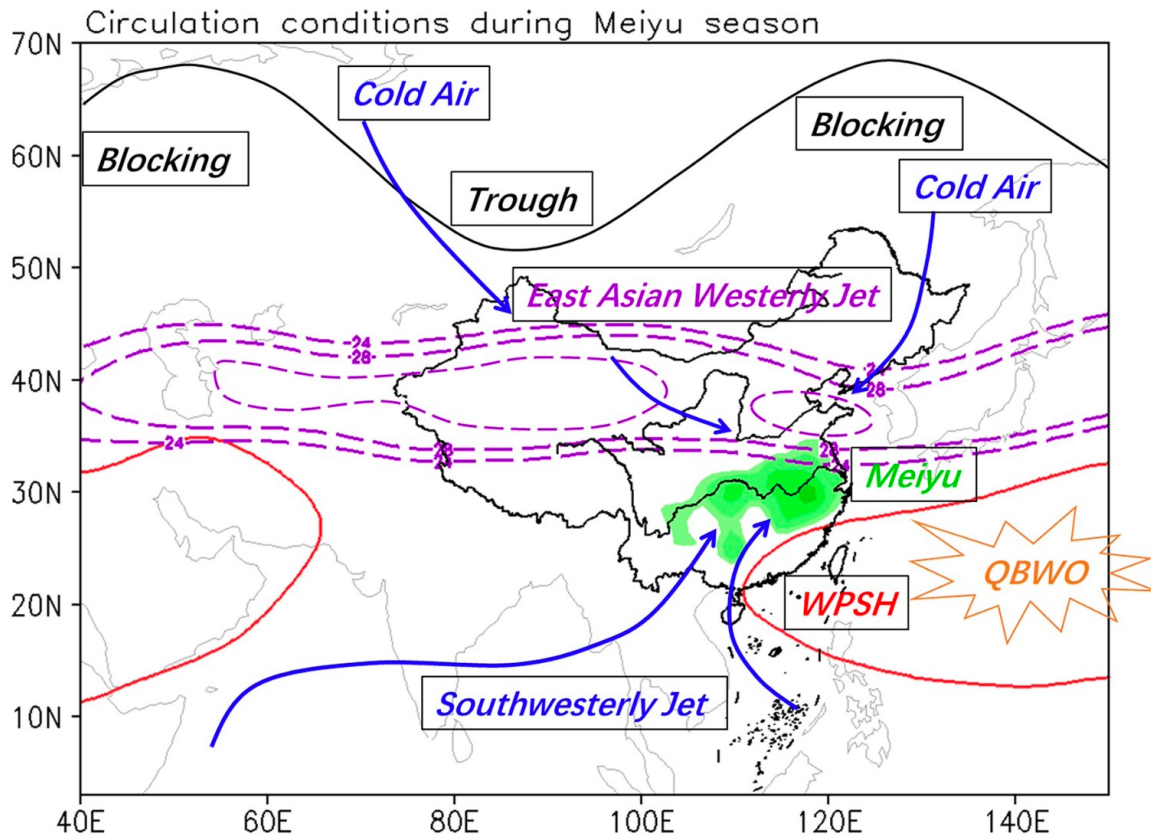


**Figure 2-6** Schematic of the causes of the extreme Mei-Yu in the summer of 2020. The red contours represent subtropical high. The purple contours represent the East Asian westerly jet. The blue arrows indicate the flow of the air masses. The black contour indicates the trough and two blocking highs. From Ding et al. (2021).

The Mei-Yu fronts are east-west quasi-stationary fronts that affect the eastern part of China around June, and are characterised by a large moisture contrast across the front but a weak temperature gradient (Zhang et al. 2018). During the Mei-Yu season in June, MCSs can occur in the Mei-Yu rainbands in eastern China for several consecutive days, bringing persistent precipitation that can lead to flooding (Guan et al. 2020). The duration, location of rainbands and intensity of precipitation of the Mei-Yu are very closely related to the East Asian monsoon circulation (Ding et al. 2021). Two of the most important environmental forcings of the Mei-

Yu are the westerly jet and the low-level southerly winds over eastern China (Sampe and Xie 2010).

In the summer of 2020, the record-breaking Mei-Yu brought severe flooding to East Asia, and the main features of this year's Mei-Yu included long duration, wide meridional rainbands, and intense precipitation (Ding et al. 2021). The total precipitation in the Yangtze River Basin in June-July 2020 is the largest in the last 20 years (Volonté et al. 2021). Ding et al. (2021) analysed the factors that contributed to the anomalous intensity of the Mei-Yu in the summer of 2020 (Figure 2-6). They revealed that the first important reason is that the East Asian monsoon circulation system exhibits pronounced quasi-biweekly oscillation (QBWO), especially the enhancement of the low-level southwesterly jet. They also revealed that another important reason is the presence of two blocking highs in the middle and high latitudes of Eurasia, which activate the trough, and the frequent southward movement of cold air masses convergence zone with warm and moist air masses, resulting in persistent heavy rainfalls. In addition to this, the MJO was anomalously quasi-stationary and active in the Indian Ocean region for 59 days from June to July 2020, bringing abundant water vapour to East Asia, which further contributed to severe heavy rainfall (Zhang et al. 2021).

## 3 Methodology

### 3.1 Dataset

Among the past studies on MCSs, most of the tracking of MCSs is based on geostationary satellite infrared brightness temperatures, which are effective for the tropics (Feng et al. 2021). But, using only geostationary satellite infrared brightness temperature to track MCS has a limitation at mid-latitudes that can incorrectly identify large cold cloud systems produced by some synoptic systems as MCSs (Feng et al. 2019). To investigate the MCS generation in East Asia more accurately, especially in the mid-latitudes of East Asia, we used a global high-resolution ( $\sim 10$  km, 1 h) MCSs tracking database from Feng et al. (2021). This database combined precipitation feature identification in addition to tracking MCSs by geostationary satellite infrared brightness temperature. Precipitation feature data were from the Global Precipitation Measurement (GPM) Integrated Multi-satellitE Retrievals (IMERG) V06B precipitation product (Tan et al. 2019; Huffman et al. 2019). The thresholds for this database to recognise MCSs are that the area of the cold cloud system is greater than  $4 \times 10^4$  km<sup>2</sup> and one axis is greater than 100 km in length; and that the precipitation feature reach the threshold requirements. These features all require longer than 4 hours. This database also excludes the effects of tropical cyclones. This database was calibrated through the radar network in the U.S. (Feng et al. 2019) and validated through the U.S. and Chinese radar networks (Feng et al. 2021). Feng et al. (2021) have shown that the method of tracking MCSs that combines precipitation feature identification and geostationary satellite infrared brightness temperature can identify MCSs for all seasons in the mid-latitudes more efficiently than a method that uses only geostationary satellite infrared brightness temperature. Here, we use this MCS tracking database to obtain the interannual variation and distributional changes in the number of MCSs in East Asia.

To investigate the relationship between environmental conditions and MCS initiation, we used the fifth generation of atmospheric reanalysis data from European Centre for Medium-Range Weather Forecasts (ECMWF) - ECMWF Reanalysis v5 (ERA5, Hersbach et al. 2020).

Here, we selected some of these environmental conditions and only selected data when the MCSs were initiated. The selected environmental conditions are described specifically in Section 3.2. The selected environmental conditions will be analysed in combination with the MCSs tracking data to analyse what environmental conditions are more related to the initiation of MCSs, and what changes in environmental conditions make the number of MCSs in East Asia change.

### **3.2 Methods of analysing environmental conditions**

To investigate the MCS environments over East Asia, we use the high-resolution MCS tracking database from Feng et al. (2021) to count the time series of the number of MCSs generated in East Asia ( $0^{\circ}$ - $55^{\circ}$ N,  $95^{\circ}$ E- $165^{\circ}$ E, see e.g., Figure 4-3) over the past two decades from 2001 to 2020. By comparison, we investigated the trend of the number of MCSs generated over the past two decades over East Asia. We selected the two years with the highest and lowest number of MCSs generated from these years and extracted the environmental conditions of these two years from ERA5 (Hersbach et al. 2020) to compare and analyse with the heat map of the distribution of the number of MCSs generated. We only selected data on the environmental conditions at the times of MCS initiation. That is, we found the initiation times of each MCS over our study region, then produced a composite environment for all initiation times.

For the selection of environmental conditions, we considered both thermodynamic and dynamic conditions. We selected convective available potential energy (CAPE) and total column water vapour (TCWV) as the thermodynamic conditions for our study. CAPE provides a good measurement of the two essential conditions for deep convection, that is, moisture and instability (Schultz et al. 2000). TCWV is a column-integrated measure of water vapour, which is a fundamental requirement for moist convection. For the dynamical conditions, we selected vertical wind shear (VWS) and vertically integrated moisture flux divergence (VIMFD). We selected three pressure intervals of VWS, which are shallow VWS (surface to 800 hPa), mid-

level VWS (800 to 600 hPa), and deep-layer VWS (surface to 600 hPa). The smaller value of VIMFD implies a stronger moisture convergence. Moisture convergence provides an ongoing supply of moisture that can maintain an MCS. The choice of these variables was informed by previous studies, which found these variables to be important for MCS formation, as discussed in Section 2.2. In order to facilitate the analysis of the relationship between the heat map of the number of MCSs and the various environmental conditions, we plotted the heat map of the differences in the number of MCSs and the contours of the differences in the environmental conditions on a single map. In addition to this, we also investigate the environmental conditions of the separated months with the aim of finding any particular months with special environmental conditions.

To investigate the MCS environments over the Mei-Yu region, we used the same methodology as in the study of environmental conditions over East Asia, but limited the study to the Mei-Yu region (25°N -37°N, 112°E-145°E, see e.g., Figure 4-13).

### **3.3 Methods of statistical analysis**

To further analyse the relationship between the number of MCSs and various environmental conditions, we calculated the spatial correlation between all variables and the MCS differences. The grid size for the number of MCSs (from the Feng et al. (2021) database) is different from the grid size for the other environmental conditions (from ERA5), so here we convert the grid for the environmental conditions to the same size as the grid for the number of MCSs by coarsening it. The environmental conditions within a single grid of the same size as the number of MCSs were averaged.

Due to the large size and varied geography of East Asia, we divided East Asia into two parts based on the results we have already obtained before, and calculated the correlation between all the variables of the two parts in turn. Then we drew the respective correlation matrices and made comparisons. For the Mei-Yu region, due to its smaller size, we only calculated the correlation for the whole and drew the correlation matrix.

## 4 Results

### 4.1 Analysis of MCS environments over East Asia

#### 4.1.1 Time series of MCS number

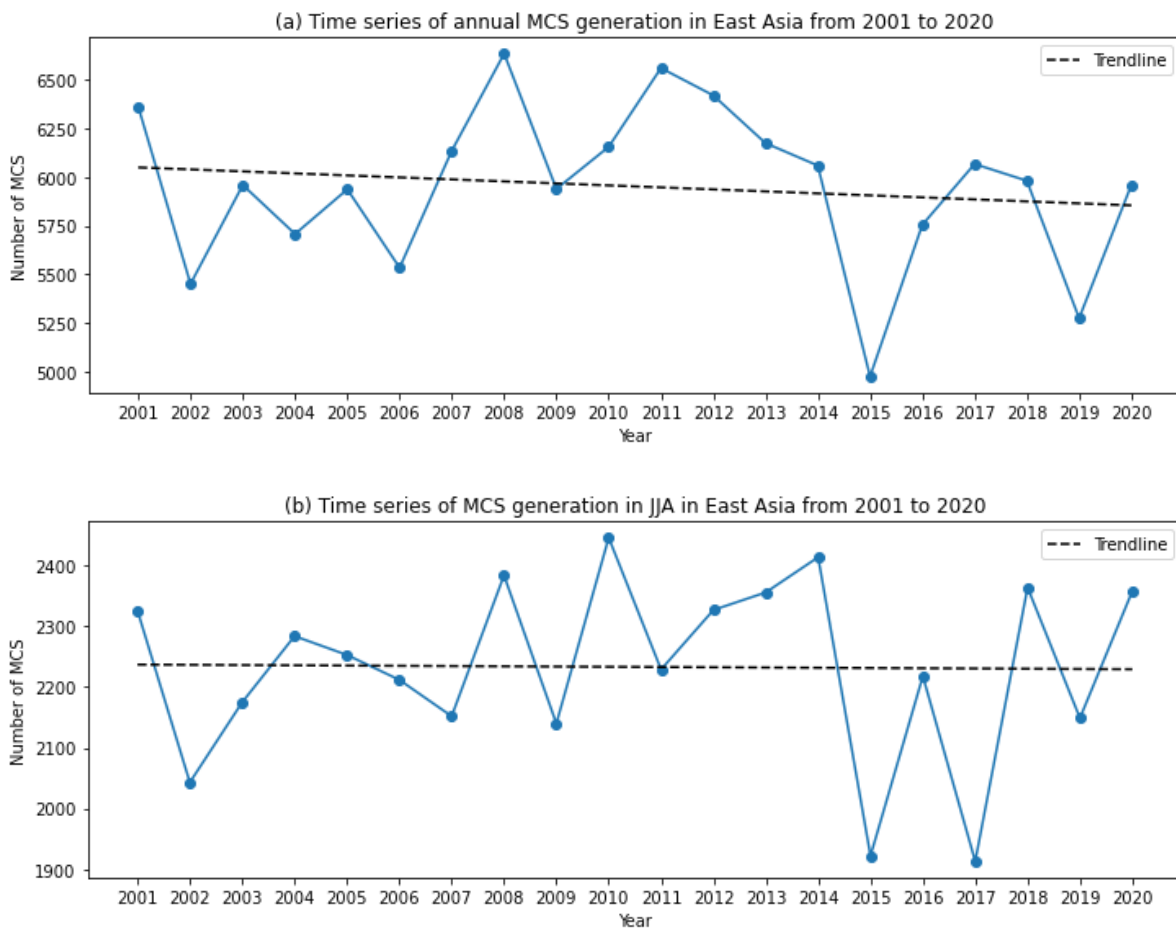
The first step of this study is to find the trend of the number of MCSs in East Asia over the last two decades and to select a pair of years with the highest and lowest number of MCSs generated for comparison.

Figure 4-1 (a) shows the time series of the number of MCSs generated in the whole year from 2001 to 2020 in East Asia. The total number of MCSs generated in East Asia for the whole period is 119,022, and the average is 5,951, with a slightly decreasing trend in general. The year with the highest number of MCSs generated is 2008, with 6,632 MCSs generated, and the year with the lowest number of MCSs generated is 2015, with 4,976.

Figure 4-1 (b) shows the time series of the number of MCSs generated in JJA from 2001 to 2020 in East Asia. The average number of MCSs generated in East Asia in JJA during the period is 2,233, which is 38% of the annual total. The overall trend is similar to that for annual mean. The year with the highest number of MCSs generated in JJA is 2010, with 2,446, and the year with the lowest number is 2017, with 1,913. In 2008, the year with the highest total annual number of MCSs, the number of MCSs generated in JJA is 2,384. In 2015, the year with the lowest total annual number of MCSs, the number of MCSs generated in JJA is 1,922.

The number of MCSs generated in JJA over East Asia accounts for 38% of the annual total. In 2008, 36% of the annual MCSs generated during JJA, and in 2015, this number was 39%. The number of MCSs generated in JJA is the highest for any three-month season, and the proportion of the total number of MCSs generated in JJA as a percentage of the year for the two years with the highest and lowest total number of MCSs generated is not meaningfully different from the mean. Hence, in analysing the environments of MCSs over East Asia, we selected only the data in JJA.

For the total number of MCSs generated for the whole year, the highest number of MCSs generated is in 2008 and the lowest is in 2015. Although the total number of MCSs generated in JJA in 2008 and 2015 are not the highest and lowest years in these two decades, respectively, they are still the two years that are meaningfully above average and meaningfully below average, respectively. While the number of MCSs generated in JJA is the highest and the lowest in 2010 and 2017, respectively, the number of MCSs generated in the whole year is close to the average in both years. Hence, we selected data for 2008 and 2015 to compare and analyse the MCS environments over East Asia.



**Figure 4-1** Time series of MCS generation in East Asia from 2001 to 2020. (a) Number of MCSs generated in the whole year; (b) number of MCSs generated in JJA.

### 4.1.2 Comparison between 2008 and 2015

After selecting 2008 and 2015 for comparison, we compared the time series of monthly MCS generation for these two years (Figure 4-2). The month with the highest number of MCSs generated in East Asia in 2008 is July with 878, and the month with the lowest number is February with 259. While the month with the highest number of MCSs generated in East Asia in 2015 is June with 688, and the month with the lowest number is March with only 178. For JJA, the main reason for the total number of MCSs generated in 2015 being meaningfully less than in 2008 is that the number of MCSs generated in July 2015 is much less than in July 2008. MCSs generated 878 in July 2008, while only 557 MCSs are generated in July 2015, which is a 37% decrease. The number of MCSs generated in July 2015 compared to June 2015 also shows a decline of 19%.

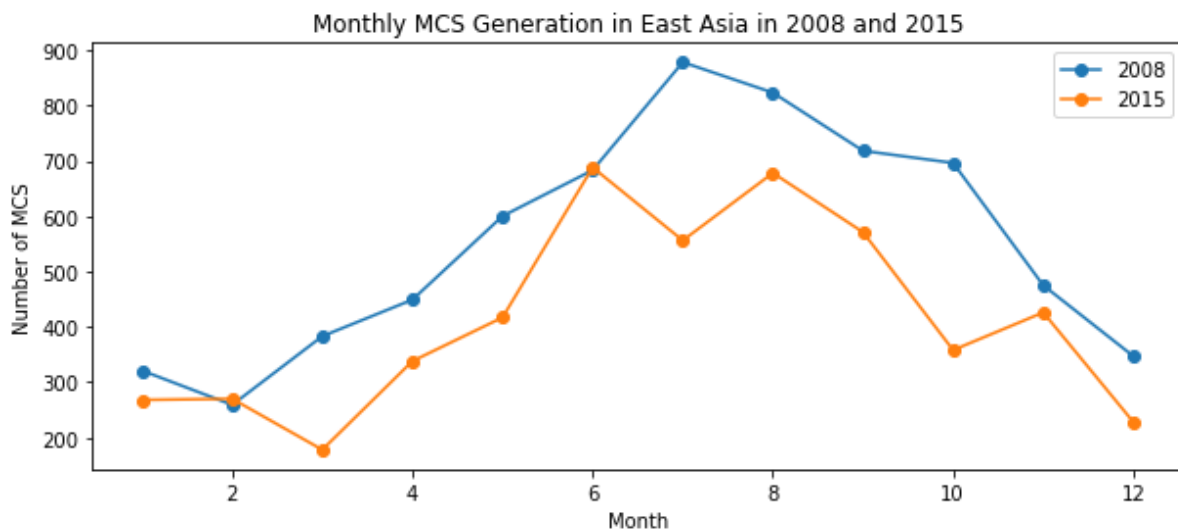


**Figure 4-2** Monthly MCS generation in East Asia in 2008 and 2015.

Following a comparison of the time series of monthly MCS generation in 2008 and 2015, we proceeded to compare the heat maps of the number of MCSs and their differences between the two years (Figure 4-3). In general, the geographical distribution of MCSs over East Asia is mainly characterised by the fact that there are more MCSs at low-latitudes than at mid-latitudes

and more MCSs in maritime regions than in continental regions (Figure 4-3 a, b, c, d).

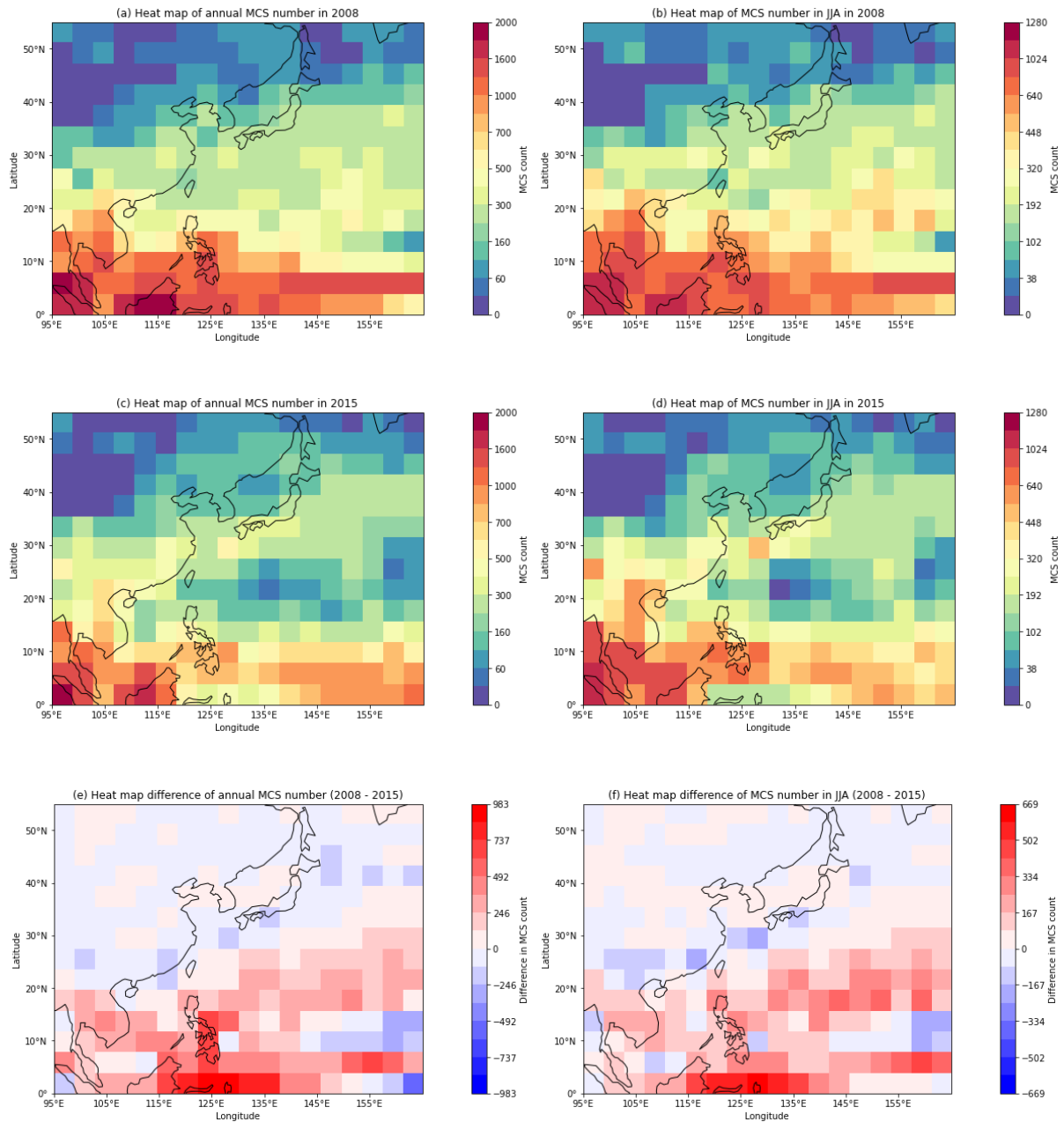


**Figure 4-3** Heat maps of MCS numbers and differences in numbers in East Asia. (a) Heat map of annual MCS number in 2008; (b) heat map of MCS number in JJA in 2008; (c) heat map of annual MCS number in 2015; (d) heat map of MCS number in JJA in 2015; (e) heat map difference of annual MCS number for 2008 minus 2015; (f) heat map difference of MCS number in JJA for 2008 minus 2015.

The heat map of the number of MCSs in JJA in 2008 has a larger proportion of MCSs than the heat map for the whole year in two regions: the region north of Palau (10°N-22°N, 130°E-140°E) and the region to the west of Wake Island and northeast of the Northern Mariana Islands (15°N-28°N, 140°E-160°E). Except for these two regions, the heat map of the number of MCSs in JJA in 2008 follows a similar pattern to the annual heat map (Figure 4-3 a, b).

The heat map of the number of MCSs in JJA in 2015 has a larger proportion in one region than the heat map for the whole year, for the region around Mindanao (5°N-15°N, 115°E-130°E). The proportion is smaller in two regions: west of Iwo Jima (20°N-28°N, 130°E-138°E) and west of the Marshall Islands (0°-10°N, 145°E-165°E). Except for these three regions, the heat map of the number of MCSs in JJA in 2008 follows a similar pattern to the annual heat map (Figure 4-3 c, d).

The heat map difference in the number of MCSs in JJA in 2008 and 2015 has a larger proportion in one region than the heat map difference for the whole year for the region to the west of Wake Island and east of the Bass Strait (15°N-25°N, 128°E-165°E). The proportion is smaller in one region around Mindanao (5°N-15°N, 120°E-130°E). The pattern of the heat map difference for JJA in 2008 and 2015 is generally similar to that of the annual heat map difference (Figure 4-3 e, f).

The heat maps for JJA are not too meaningfully different from the annual heat maps, which share a similar pattern. Hence it is justified to use the data in JJA to replace the annual data to study.

In terms of the heat map difference in the number of MCSs in JJA between 2008 and 2015, the number of MCSs in 2008 is larger than that in 2015 in most regions, especially in the region around Mindanao (0°-20°N, 115°E-140°E), the region west of Wake Island and east of Bass Strait (15°N-30°N, 130°E-165°E), and the region west of the Marshall Islands (5°N-8°N, 140°E-165°E). Two regions with fewer MCSs in 2008 than in 2015 are the region northwest of the Marshall Islands (7°N-15°N, 155°E-165°E) and the region along the southern China-East China Sea-Japan line (Figure 4-3 f).

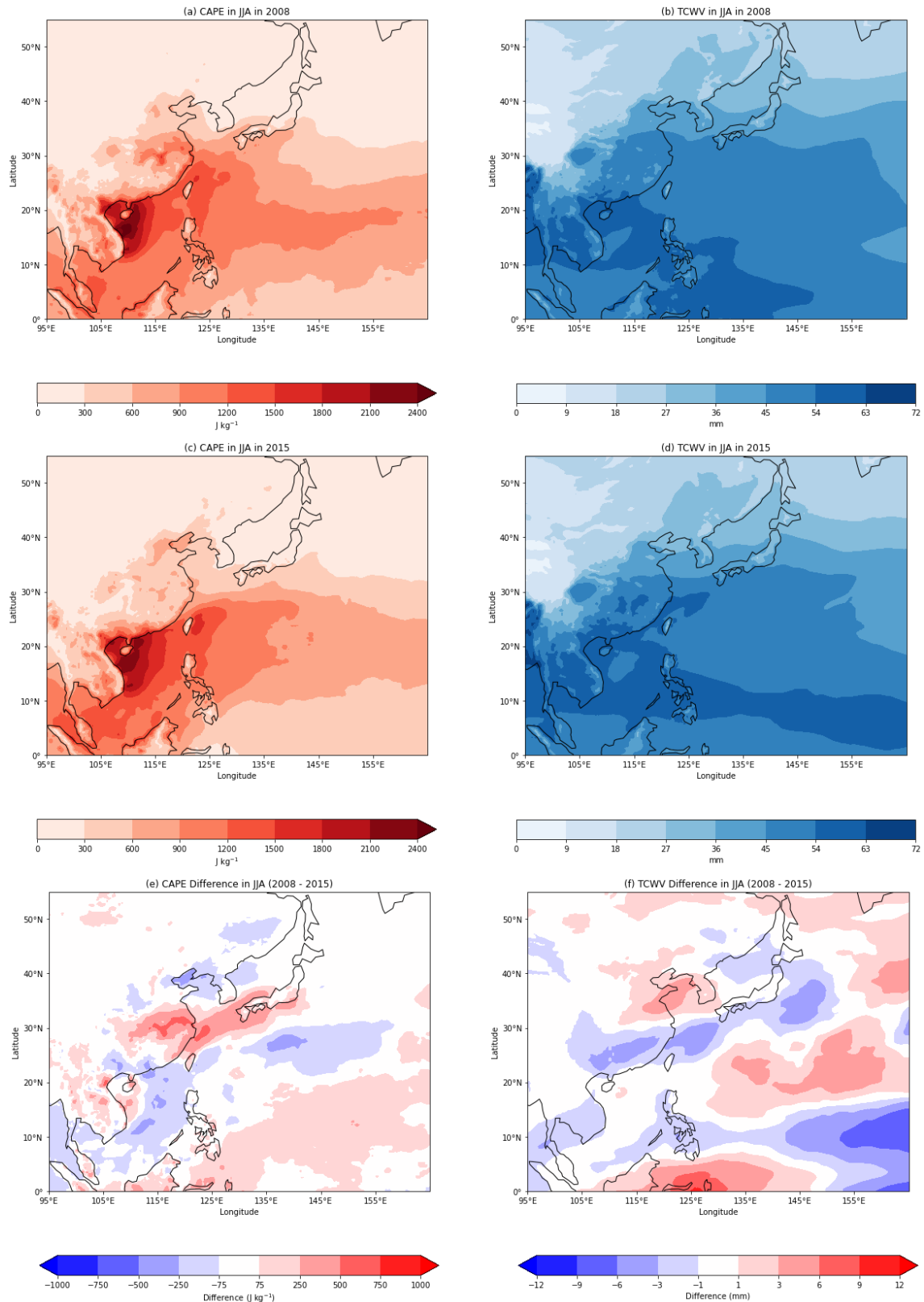
When compared to each other, there are clear differences in MCS initiation between 2008 and 2015, both annually and over JJA. The spatial pattern of these differences indicates that there may be environmental conditions that control the number of MCSs occurring in both years and which may explain the differences.

### **4.1.3 Analysis of thermodynamic conditions**

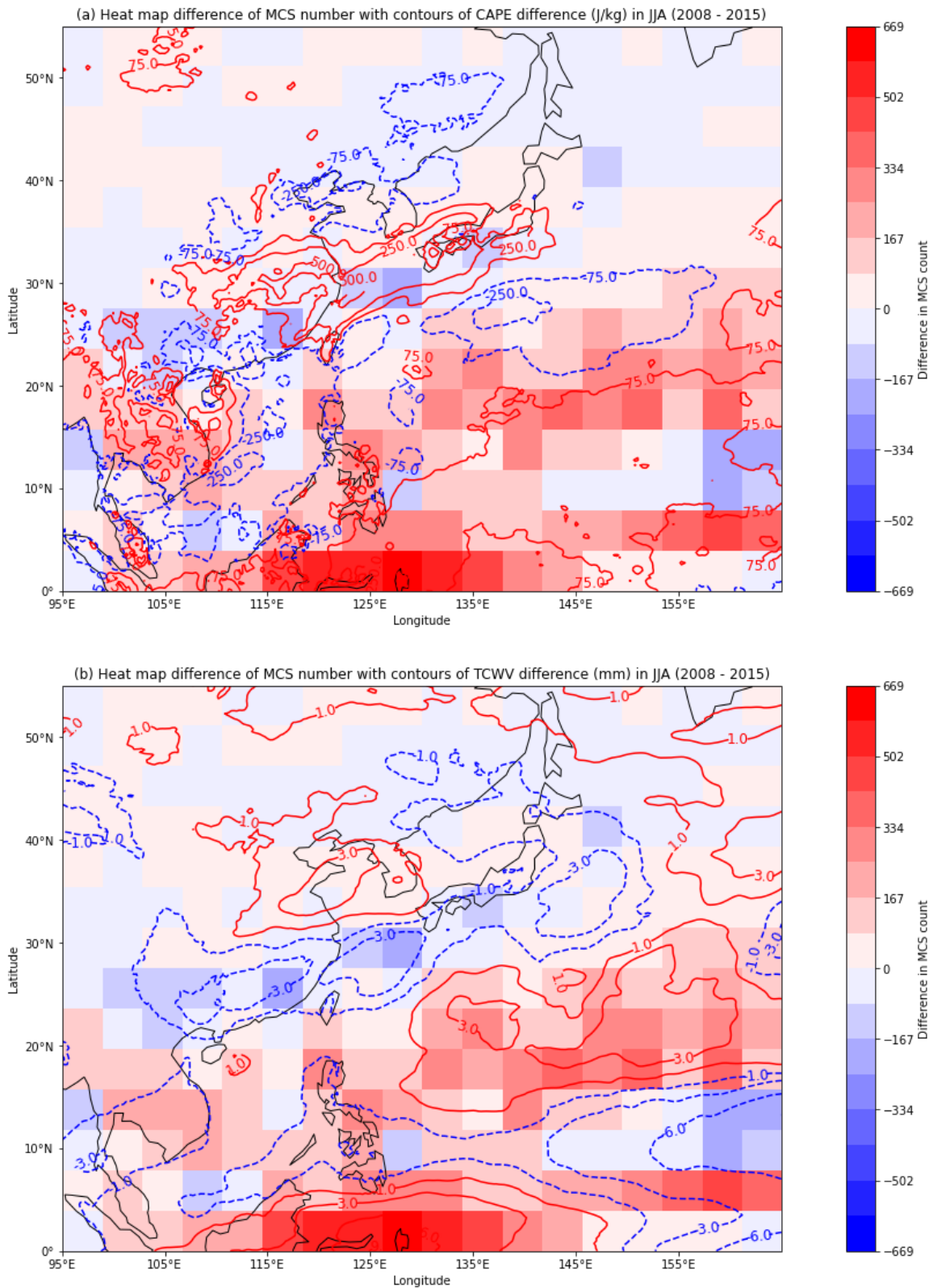
In Section 4.1.2, we found that there may be some environmental conditions controlling the number of MCSs, here we first analysed the thermodynamic conditions. We selected CAPE and TCWV to analyse the thermodynamic conditions and the reasons for this were stated in Sections 2.2 and 3.2.

Figure 4-4 shows the distribution of CAPE and TCWV over East Asia in 2008 and 2015 and differences between the two years, composited on MCS initiation over the region. There is some consistency in the distribution of CAPE and TCWV in 2008 and 2015, which is particularly evident in the South China Sea (Figure 4-4 a, b, c, d). In both 2008 and 2015, the area with the most CAPE is near Hainan Island (Figure 4-4 a, c). But the distribution of the difference in CAPE and the difference in TCWV is quite different between 2008 and 2015 (Figure 4-4 e, f).

By analysing the differences in CAPE at the times of MCS initiation over East Asia between 2008 and 2015, we found the following regions where these differences were more substantial (Figure 4-4, e). The two main regions where CAPE is substantially higher in 2008 than in 2015 are the region along the Indo-China Peninsula and the western part of the South China Sea (13°N-20°N, 100°E-112°E) and the region along the eastern China-East China Sea-Japan line (24°N-35°N, 105°E-140°E). The three main regions where the CAPE in 2008 is substantially lower than that in 2015 are the region around the Bohai Sea (35°N-42°N, 117°E-125°E), the region around the eastern part of the South China Sea (7°N-22°N, 112°E-122°E), and the region around the southern part of Japan (20°N-30°N, 132°E-157°E).



**Figure 4-4** Distribution of CAPE and TCWV at the times of MCS initiation over East Asia in JJA in 2008 and 2015 and differences between the two years. (a) CAPE in JJA 2008; (b) TCWV in JJA 2008; (c) CAPE in JJA 2015; (b) TCWV in JJA 2015; (e) CAPE difference in JJA between 2008 and 2015 (2008 - 2015); (f) TCWV difference in JJA between 2008 and 2015 (2008 - 2015).



**Figure 4-5** Heat map differences in the number of MCSs between 2008 and 2015 with contours of the CAPE and TCWV differences over East Asia for both years. (a) The heat map with contours of the CAPE difference (2008 - 2015); (b) the heat map with contours of the TCWV difference (2008 - 2015).

By analysing the differences in TCWV at the times of MCS initiation over East Asia between 2008 and 2015, we found the following regions where these differences were more substantial (Figure 4-4, f). The three main regions with substantially higher TCWV in 2008 than in 2015 are the region along the Huanghai Sea ( $30^{\circ}\text{N}$ - $40^{\circ}\text{N}$ ,  $115^{\circ}\text{E}$ - $130^{\circ}\text{E}$ ), the region from east of the Bass Strait to west of Wake Island ( $15^{\circ}\text{N}$ - $28^{\circ}\text{N}$ ,  $130^{\circ}\text{E}$ - $165^{\circ}\text{E}$ ), and the region along the south of Mindanao ( $0^{\circ}$ - $5^{\circ}\text{N}$ ,  $110^{\circ}\text{E}$ - $145^{\circ}\text{E}$ ). The three main regions where the TCWV in 2008 is substantially lower than that in 2015 are the region along the southern China-East China Sea line ( $20^{\circ}\text{N}$ - $30^{\circ}\text{N}$ ,  $105^{\circ}\text{E}$ - $130^{\circ}\text{E}$ ), the region around southeastern Japan ( $27^{\circ}\text{N}$ - $40^{\circ}\text{N}$ ,  $140^{\circ}\text{E}$ - $150^{\circ}\text{E}$ ), and the region around the west of the Marshall Islands ( $0^{\circ}$ - $15^{\circ}\text{N}$ ,  $145^{\circ}\text{E}$ - $165^{\circ}\text{E}$ ).

By comparing MCS frequency against MCS initiation composite environments, we found that the number of MCSs generated in East Asia is not related to CAPE (Figure 4-5 a). In some regions where the value of the CAPE difference is positive, the difference in the number of MCSs generated is negative. For example, the region along the East China Sea ( $25^{\circ}\text{N}$ - $32^{\circ}\text{N}$ ,  $115^{\circ}\text{E}$ - $135^{\circ}\text{E}$ ) has a larger CAPE in 2008 than in 2015, but has a smaller number of MCSs generated. In some regions where the value of the CAPE difference is negative, the difference in the number of MCSs generated is positive. For example, the region around the southern part of the South China Sea ( $5^{\circ}\text{N}$ - $20^{\circ}\text{N}$ ,  $110^{\circ}\text{E}$ - $120^{\circ}\text{E}$ ) has a smaller CAPE in 2008 than in 2015, but has a higher number of MCSs generated. This suggests that CAPE may not be a strong predictor for MCS initiation, at least for these two years.

However, when we compared the relationship between TCWV and the number of MCSs generated, we found a similar pattern between the two (Figure 4-5 b). The contours of the TCWV differences are consistent with much of the heat map differences in number of MCSs generated. In the region south of Mindanao ( $0^{\circ}$ - $5^{\circ}\text{N}$ ,  $115^{\circ}\text{E}$ - $140^{\circ}\text{E}$ ), TCWV is higher in 2008 than in 2015, and similarly, in this region, the number of MCSs generated in 2008 is much higher than in 2015. The same link is also found in the region from east of Bass Strait to west of Wake Island ( $15^{\circ}\text{N}$ - $28^{\circ}\text{N}$ ,  $130^{\circ}\text{E}$ - $165^{\circ}\text{E}$ ). Similarly, in the region along the southern China-East China Sea-southern Japan line ( $20^{\circ}\text{N}$ - $35^{\circ}\text{N}$ ,  $105^{\circ}\text{E}$ - $150^{\circ}\text{E}$ ), the TCWV is substantially lower in 2008 than in 2015, and in this region, the number of MCSs generated in 2008 is also substantially less than in 2015. The same link is also seen in the region along the west of the

Marshall Islands ( $0^{\circ}$ - $15^{\circ}$ N,  $145^{\circ}$ E- $165^{\circ}$ E). This relationship does not hold everywhere. Close to  $10^{\circ}$ N,  $125^{\circ}$ E- $140^{\circ}$ E there is lower TCWV in 2008 than 2015. However, there are marginally more MCSs in this region in 2008. Despite this, overall TCWV seems to be a good predictor for understanding the differences between MCS initiation between the two years.

#### **4.1.4 Analysis of dynamic conditions**

After comparing the thermodynamic conditions, we proceeded to compare the dynamical conditions. In this study, we selected VWS and VIMFD as the thermodynamic conditions to be analysed and the reasons were stated in Sections 2.2 and 3.2 as well. We selected three pressure intervals of VWS, which are shallow VWS (surface to 800 hPa), mid-level VWS (800 to 600 hPa), and deep-layer VWS (surface to 600 hPa). All VWS and VIMFD below refer to VWS and VIMFD at the times of MCS initiation.

In the region around the East China Sea ( $23^{\circ}$ N- $32^{\circ}$ N,  $122^{\circ}$ E- $135^{\circ}$ E) and in the region to the west of Japan ( $30^{\circ}$ N- $50^{\circ}$ N,  $143^{\circ}$ E- $165^{\circ}$ E), the VWS over all three pressure intervals is substantially weaker in 2008 than in 2015 (Figure 4-6 a, b, c). The mid-level VWS is also substantially weaker in the middle and lower reaches of the Yangtze River Basin in China ( $25^{\circ}$ N- $35^{\circ}$ N,  $105^{\circ}$ E- $120^{\circ}$ E) in 2008 than in 2015, but not meaningfully different for the other two intervals. The shallow VWS in 2008 is much weaker in the region south of Mindanao ( $0^{\circ}$ - $10^{\circ}$ N,  $120^{\circ}$ E- $130^{\circ}$ E) than in 2015 (Figure 4-6 a). The mid-level VWS in 2008 is much weaker in the region west of the Marshall Islands ( $0^{\circ}$ - $10^{\circ}$ N,  $130^{\circ}$ E- $165^{\circ}$ E) than in 2015 (Figure 4-6 b). And the deep-layer VWS is meaningfully different in both regions (Figure 4-6 c).

In the northern part of China ( $40^{\circ}$ N- $55^{\circ}$ N,  $95^{\circ}$ E- $135^{\circ}$ E), VWS is substantially stronger in 2008 than in 2015 at all three intervals. Also, VWS at all three intervals in the South China Sea ( $10^{\circ}$ N- $20^{\circ}$ N,  $110^{\circ}$ E- $120^{\circ}$ E) and northwest of Wake Island ( $20^{\circ}$ N- $30^{\circ}$ N,  $150^{\circ}$ E- $165^{\circ}$ E) is stronger in 2008 than in 2015.

As shown in Figure 4-6 (d), three regions have substantially lower VIMFD in 2008 than

in 2015, namely the region north of the South China Sea (17°N-22°N, 110°E-120°E), the region south of Mindanao (0°-5°N, 110°E-145°E), and the region northwest of Wake Island (18°N-28°N, 150°E-165°E). Two regions have substantially higher VIMFD in 2008 than in 2015: the region around the East China Sea (23°N-33°N, 120°E-135°E), and the region northeast of Palau to the west of the Marshall Islands (5°N-15°N, 140°E-165°E).

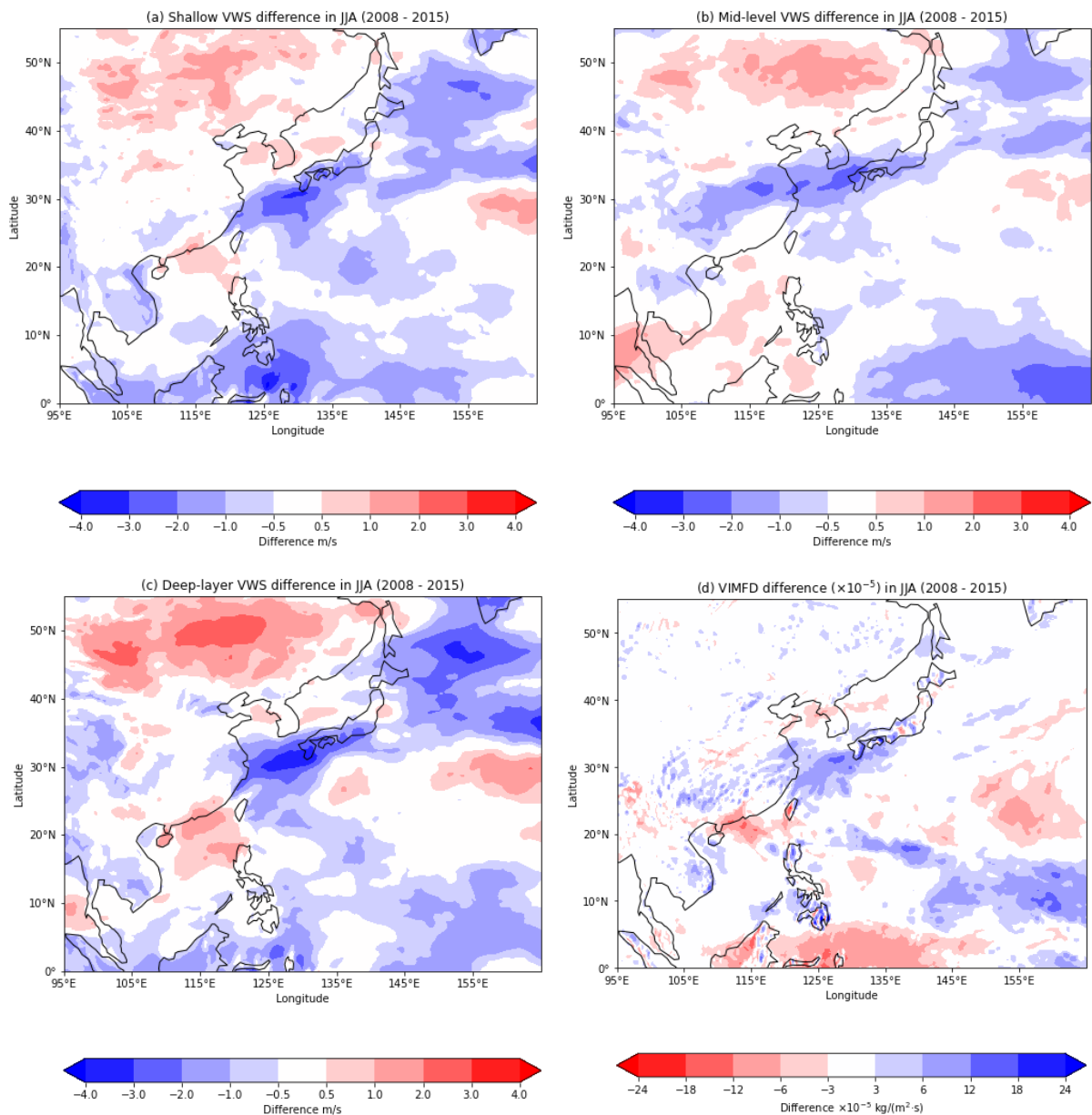


**Figure 4-6** Distribution of VWS difference and VIMFD difference at the times of MCS initiation over East Asia in JJA between 2008 and 2015. (a) Shallow VWS difference (2008 - 2015); (b) Mid-level VWS (2008 - 2015); (c) Deep-layer VWS difference (2008 - 2015); (b) VIMFD difference between two years (2008 - 2015).

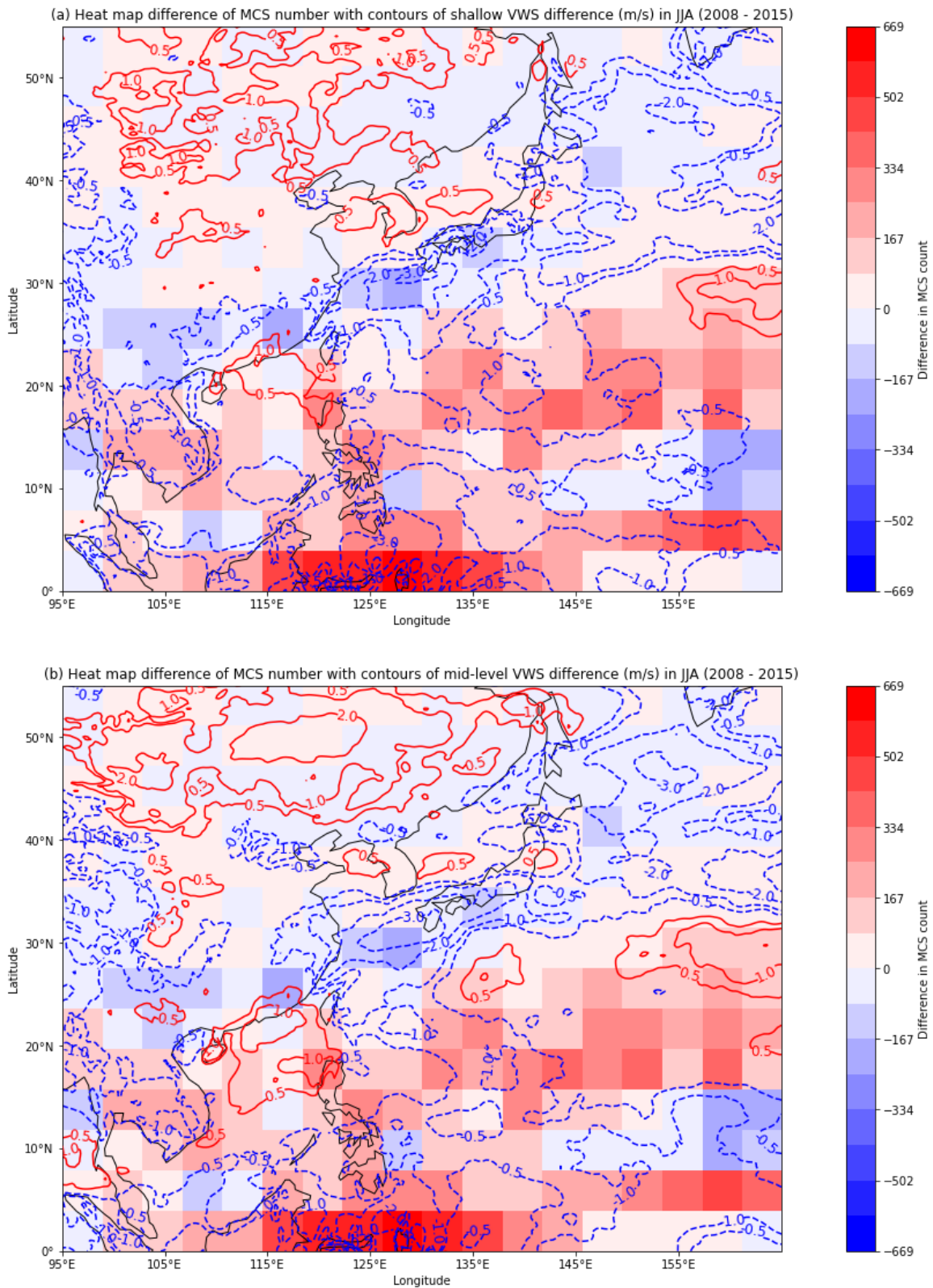


**Figure 4-7** Heat map differences of MCS number between 2008 and 2015 with contours of VWS and VIMFD differences at the times of MCS initiation. (a) Heat map difference with contours of the shallow VWS difference (2008 - 2015); (b) Heat map difference with contours of the mid-level VWS difference (2008 - 2015).

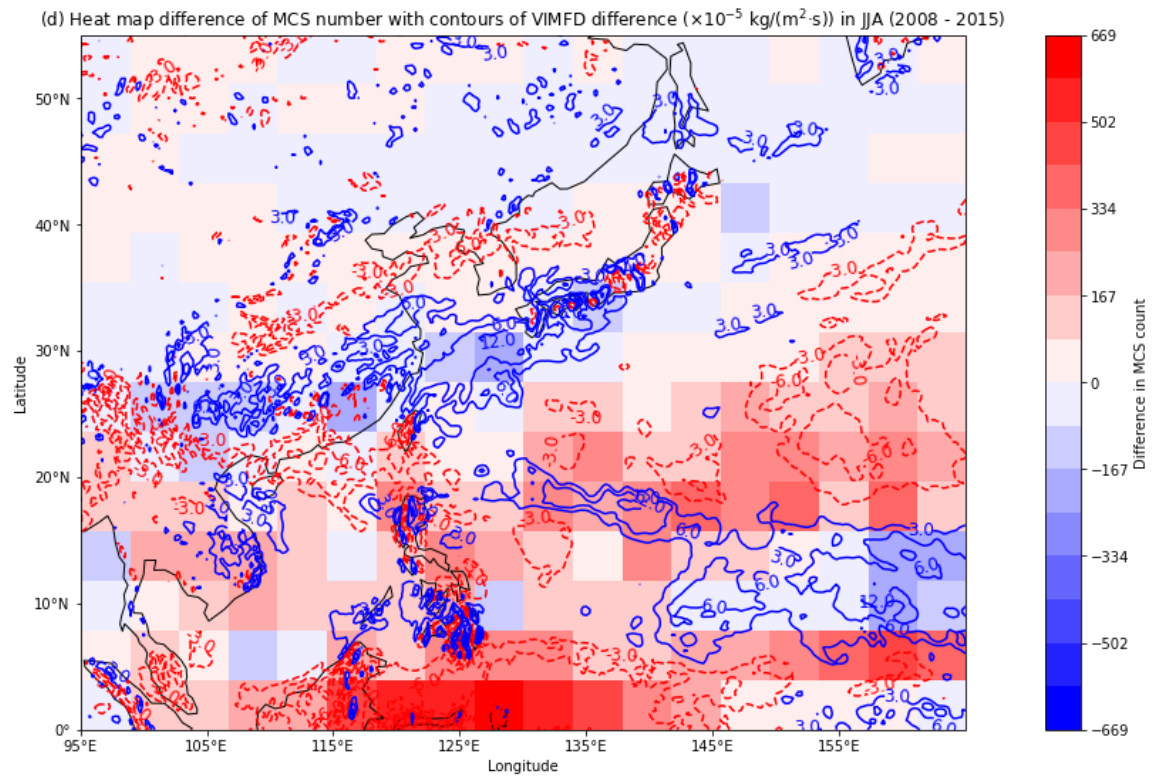
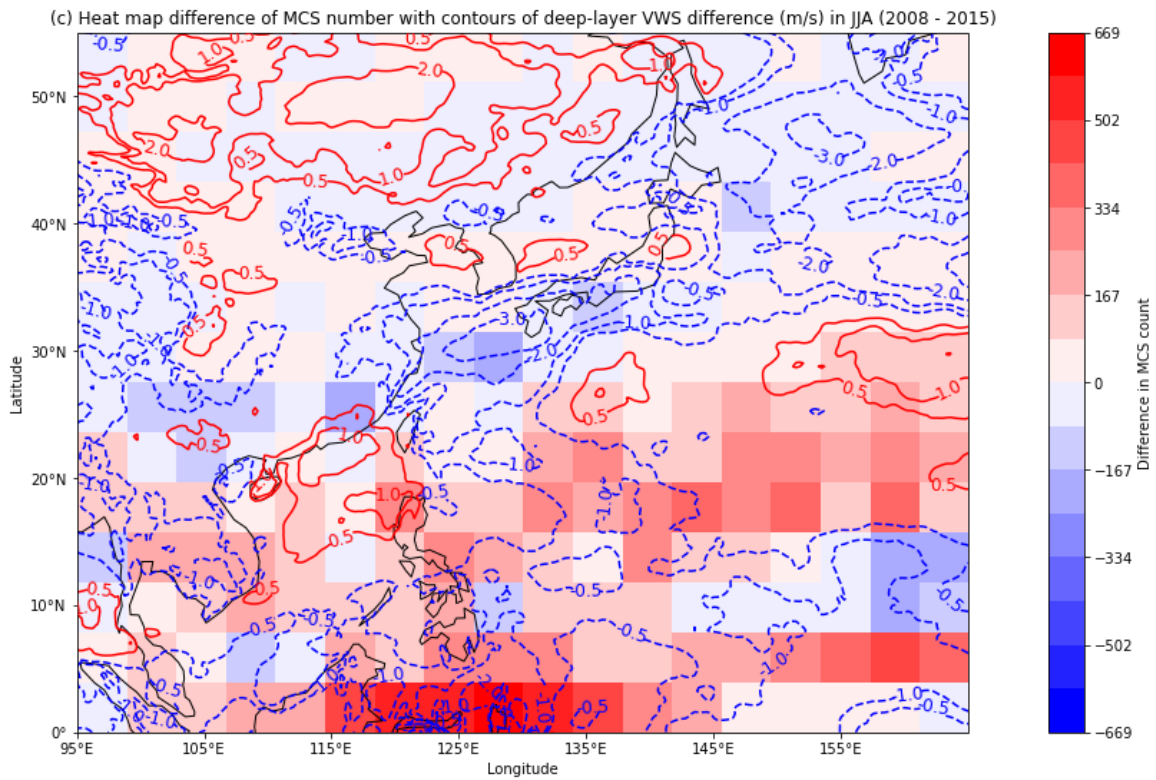


**Figure 4-7** Heat map differences of MCS number between 2008 and 2015 with contours of the VWS and VIMFD differences at the times of MCS initiation. (c) Heat map difference with contours of the deep-layer VWS difference (2008 - 2015); (d) Heat map difference with contours of the VIMFD difference (2008 - 2015)

The pattern of the differences in VIMFD and the differences in VWS at the three intervals are similar at low and middle latitudes ( $10^{\circ}\text{N}$ - $40^{\circ}\text{N}$ ). However, the patterns do not match near the equator ( $0^{\circ}$ - $5^{\circ}\text{N}$ ) and at mid- to high-latitudes ( $40^{\circ}\text{N}$ - $55^{\circ}\text{N}$ ).

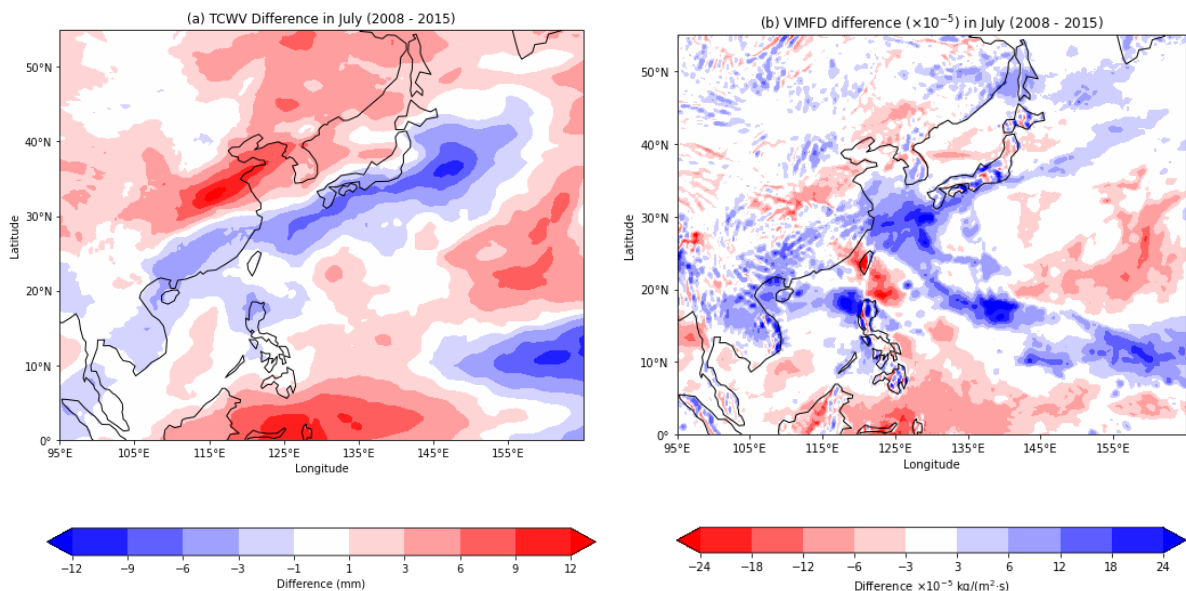
By comparing the difference in VWS at the three intervals with the heat map differences of MCS number (Figure 4-7 a, b, c), the patterns of the two do not match in the tropics ( $0^{\circ}$ - $25^{\circ}\text{N}$ ), but do match outside of that ( $25^{\circ}\text{N}$ - $55^{\circ}\text{N}$ ). For example, VWS in 2008 in the region south of Mindanao ( $0^{\circ}$ - $5^{\circ}\text{N}$ ,  $110^{\circ}\text{E}$ - $145^{\circ}\text{E}$ ) is weaker than in 2015, yet there are more MCSs in this region in 2008. VWS in the northern part of the South China Sea ( $17^{\circ}\text{N}$ - $22^{\circ}\text{N}$ ,  $110^{\circ}\text{E}$ - $120^{\circ}\text{E}$ ) is stronger in 2008 than in 2015, yet there are fewer MCSs in this region in 2008. In contrast, in the middle and high latitudes, VWS in the region along the eastern China-East China Sea-Japan line ( $25^{\circ}\text{N}$ - $35^{\circ}\text{N}$ ,  $115^{\circ}\text{E}$ - $150^{\circ}\text{E}$ ) is weaker in 2008 than in 2015, and similarly, there are fewer MCSs in this region in 2008. VWS in the region north-west of Wake Island ( $20^{\circ}\text{N}$ - $30^{\circ}\text{N}$ ,  $150^{\circ}\text{E}$ - $165^{\circ}\text{E}$ ) is stronger in 2008 than in 2015, and similarly, there are more MCSs in this region in 2008. This suggests that VWS may be a better predictor of MCS initiation at higher latitudes, but not at lower latitudes.

Figure 4-7 (d) has some noise in the contours of the differences in VIMFD, but it is nonetheless clear that the patterns of the VIMFD differences and the heat map differences of the number of MCSs are similar. For example, the lower VIMFD in 2008 than in 2015 in the southern region of Mindanao ( $0^{\circ}$ - $5^{\circ}\text{N}$ ,  $110^{\circ}\text{E}$ - $145^{\circ}\text{E}$ ) and in the northwestern region of Wake Island ( $20^{\circ}\text{N}$ - $30^{\circ}\text{N}$ ,  $150^{\circ}\text{E}$ - $165^{\circ}\text{E}$ ) implies that there is more convergence in these two regions, which is consistent with the fact that there are more MCSs in these two regions in 2008. The higher VIMFD in 2008 than in 2015 in the region west of the Marshall Islands ( $5^{\circ}\text{N}$ - $15^{\circ}\text{N}$ ,  $140^{\circ}\text{E}$ - $165^{\circ}\text{E}$ ) and in the region around the East China Sea ( $23^{\circ}\text{N}$ - $33^{\circ}\text{N}$ ,  $120^{\circ}\text{E}$ - $135^{\circ}\text{E}$ ) implies that there is more divergence in these two regions, which is consistent with the fact that there are fewer MCSs in these two regions in 2008. Thus, VIMFD shows some potential for understanding the differences in MCS initiation between the two years.

### 4.1.5 Analysis of individual months

In Section 4.1.2, we found that there is a big difference in the number of MCSs generated in the month of July between the two years 2008 and 2015. In Figure 4-3, we found that the region with the largest number of MCSs in 2008 than in 2015 is the region south of Mindanao ( $0^{\circ}$ - $5^{\circ}$ N,  $110^{\circ}$ E- $145^{\circ}$ E). Additionally, in Sections 4.1.3 and 4.1.4 respectively, we also found that the pattern of differences in TCWV and the pattern of differences in VIMFD are both similar to the pattern of the heat map differences of the number of MCSs.

In order to further investigate these findings, we plotted the MCS-initiation composite TCWV difference and the MCS-initiation composite VIMFD difference in July between 2008 and 2015 (Figure 4-8). We find that TCWV in 2008 is much higher than in 2015 for the region south of Mindanao (Figure 4-8 a). VIMFD in 2008 is much higher than in 2015 for the region south of Mindanao (Figure 4-8 b). These two patterns of environmental conditions are consistent with Figure 4-4 (f) and Figure 4-6 (d), suggesting that there is not much intra-seasonal variation in JJA.



**Figure 4-8** Differences of environmental conditions at the times of MCS initiation in July between 2008 and 2015 (2008 -2015). (a) TCWV; (b) VIMFD.

### 4.1.6 Correlation analysis

In Sections 4.1.3 and 4.1.4, we analysed thermodynamic conditions and dynamic conditions, respectively, and in this section, we used a more statistical method. To further investigate the relationship between all the variables, we calculated the correlation between each variable and plotted the correlation matrix (Figure 4-9). It should be emphasised that all environmental conditions are MCS-initiation composite environmental conditions.

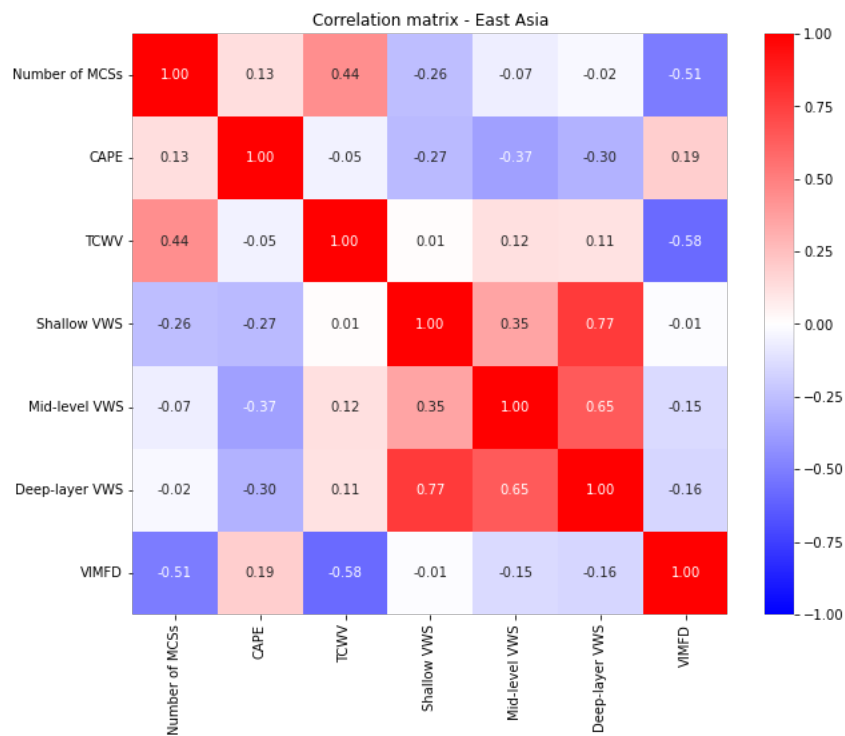


**Figure 4-9** Correlation matrix of the number of MCSs and various environmental conditions over East Asia.

In East Asia, the variable most strongly associated with the number of MCSs is VIMFD, with a correlation coefficient of -0.51. The correlation coefficient between VIMFD and number of MCSs is negative due to the fact that VIMFD is divergence and MCS generation is favoured by more convergence. The variable second most strongly associated with the number of MCSs is TCWV, with a correlation coefficient of 0.44. As expected, TCWV and VIMFD are strongly

negatively correlated. However, the higher correlation between VIMFD and the number of MCSs suggests that the dynamical component of VIMFD plays a small but important part. The variable with the smallest relationship to the number of MCSs is deep-layer VWS, with a correlation coefficient of only -0.02. This implies that the MCS initiation composite environmental conditions that are most relevant to MCSs in East Asia are TCWV and vertically integrated moisture flux convergence, and there is little relevance to deep-layer VWS.

Between the different environmental conditions, deep-layer VWS contains two other intervals: deep-layer VWS is more closely related to both shallow VWS and mid-level VWS. The correlation coefficient between shallow VWS and deep-layer VWS is larger, with a value of 0.77, which shows that shallow VWS is dominant among deep-layer VWS.

In Section 4.1.4, we found that different intervals of VWS showed different relationships with the number of MCSs at low and mid-latitudes over East Asia. Hence, we used 28°N as the boundary and divided East Asia into 0°-28°N and 28°N-55°N, and calculated correlation coefficients and plotted correlation matrices for the number of MCSs and all environmental conditions in the two regions, respectively (Figure 4-10).

As shown in Figure 4-10 (a), the correlation coefficient between TCWV and the number of MCSs is the largest in terms of the relationship between environmental conditions and the number of MCSs in the low latitude range of 0°-28°N over East Asia, with a value of 0.65. The second largest correlation coefficient between environmental conditions and the number of MCSs is for VIMFD, with a value of -0.51. The environmental condition with the smallest relationship with MCSs is mid-level VWS, with a correlation coefficient of only -0.07. The largest correlation coefficients between the different environments remain the same for TCWV and VIMFD, with a value of -0.67, which is larger in absolute value than the absolute value of the correlation coefficients for the entire East Asian range. For the different intervals of VWS, shallow VWS and mid-level VWS show a weak relationship with a correlation coefficient of only 0.12.

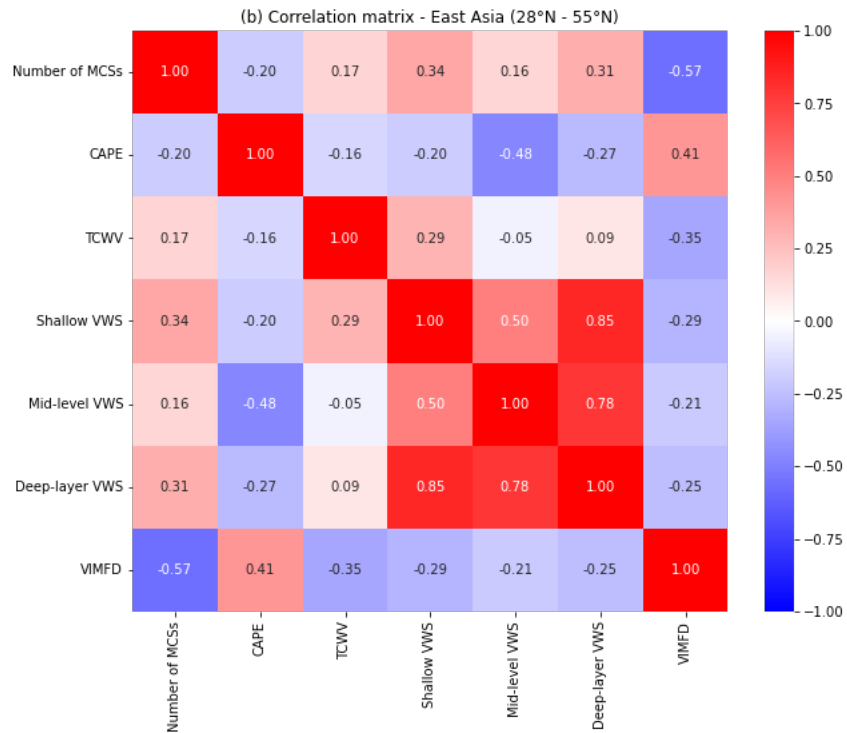
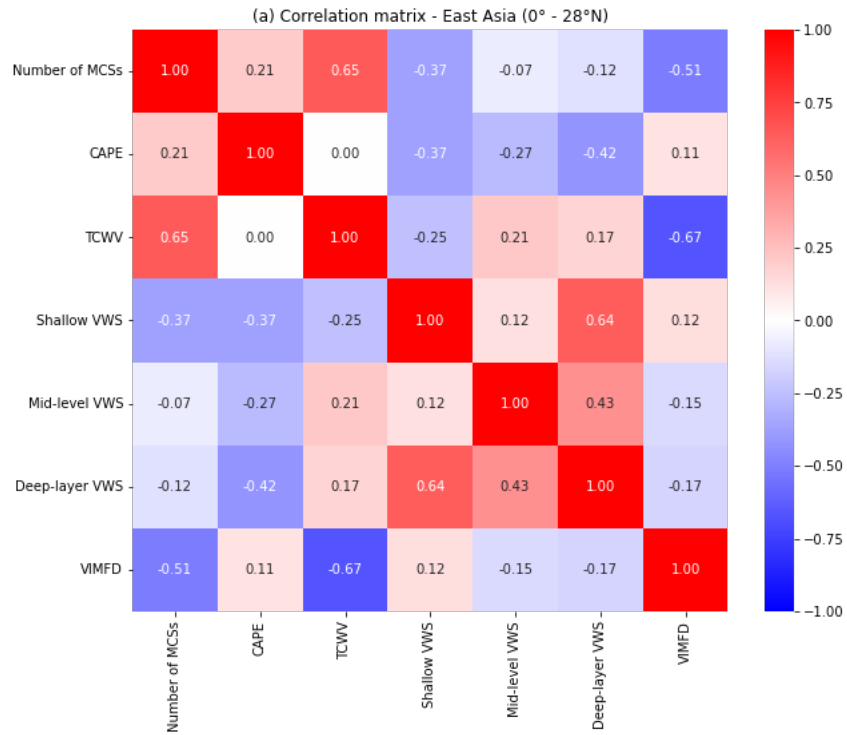


**Figure 4-10** Correlation matrix of the number of MCSs and various environmental conditions in two different regions of East Asia. (a) 0° - 28°N; (b) 28°N - 55°N.

As shown in Figure 4-10 (b), the correlation coefficient between VIMFD and the number of MCSs is the largest in terms of the relationship between environmental conditions and the number of MCSs in the mid-latitude range of 28°N-55°N over East Asia, with a value of -0.57. What is surprising is that the correlation coefficient between TCWV and the number of MCSs is only 0.17 at 28°N-55°N, which is considerably lower compared to the correlation coefficient of 0.65 at 0°-28°N. This suggests that the dynamical component of VIMFD becomes more important at higher latitudes.

Another surprising thing is that the correlation coefficient between the number of MCSs and shallow VWS changes from -0.37 for 0°-28°N to 0.34 for 28°N-55°N. Remarkably, the relationship between the number of MCSs and shallow VWS shows almost opposite relationships at 0°-28°N and 28°N-55°N. The correlation coefficient between the number of MCSs and deep-layer VWS also increases to 0.31. Among the relationships between different environmental conditions, the three different intervals of VWS show a stronger link between 28°N-55°N over East Asia. CAPE also shows a stronger association with mid-level VWS with a correlation coefficient of -0.48. Also, there is a stronger relationship between CAPE and VIMFD at 28°N-55°N than at 0°-28°N, with a correlation coefficient of 0.41. These facts are discussed in Section 5.2.

## **4.2 Analysis of MCS environments over the Mei-Yu region**

During the summer months, quasi-stationary Mei-Yu fronts are formed in the Mei-Yu region (25°N-37°N, 112°E-145°E), in which large amounts of MCSs are produced. The Mei-Yu region has a large population density, and MCSs have a high impact on this region. Thus, we limited our domain to the Mei-Yu region of East Asia to investigate environmental conditions.

### 4.2.1 Time series of MCS number

The Mei-Yu region covers 10% of the area of East Asia, and the number of MCSs generated by the Mei-Yu region in JJA is also 10% of all of East Asia (Figure 4-1 b, Figure 4-11 b). Since the number of MCSs generated at low latitudes is much larger than that at mid-latitudes, and the Mei-Yu region is located in the mid-latitudes. The fact that there is the same percentage of the number of MCSs in JJA as the percentage of the area already indicates the high number of MCSs generated in JJA over the Mei-Yu region.

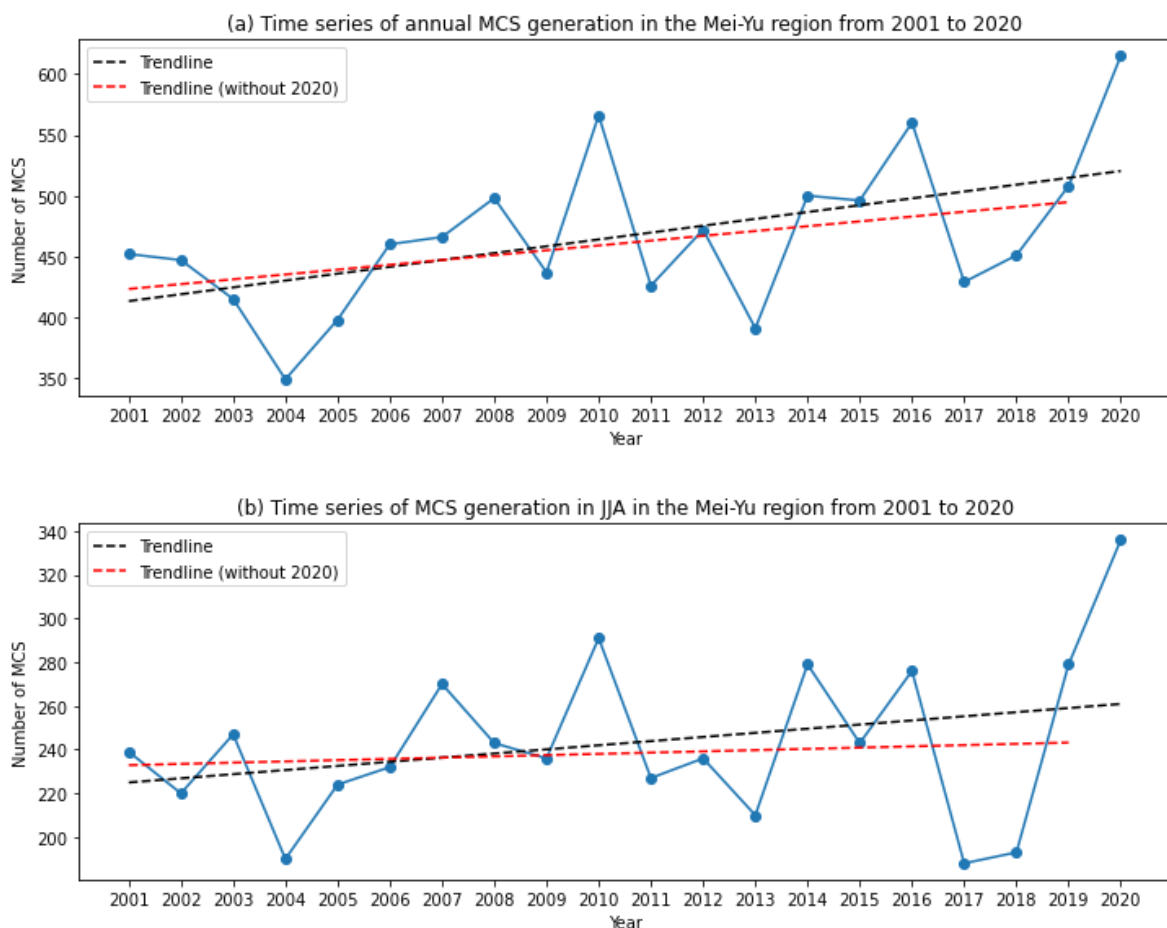
Figure 4-11 (a) shows the time series of the number of MCSs generated in the whole year from 2001 to 2020 in the Mei-Yu region. The total number of MCSs generated in the Mei-Yu region for the whole period is 9,336, and the average is 467, with an increasing trend in general. The year with the highest number of MCSs generated in a whole year is 2020, with 615, and the year with the lowest number is 2004, with 349. The case of 2020 is more extreme, so we additionally fitted only the data from 2001-2019 and found that the number of MCSs in the Mei-Yu region continued to show an increasing trend for the whole year. This suggests a strong long-term increasing trend in the number of MCSs for the whole year in the Mei-Yu region.

Figure 4-11 (b) shows the time series of the number of MCSs generated in JJA from 2001 to 2020 in the Mei-Yu region. The total number of MCSs generated in the Mei-Yu region in JJA from 2001 to 2020 is 4,859, and the average is 243, with an increasing trend in general. The year with the highest number of MCSs generated in JJA is 2020, with 336, and the year with the lowest number is 2017, with 188. In 2004, the year with the lowest total annual number of MCSs generated, the number of MCSs generated in JJA is 190. We fitted the number of MCSs generated in JJA in the Mei-Yu region after excluding the 2020 data as we did for the whole year. The result shows a stable trend of the number of MCSs in JJA in the Mei-Yu region after removing the 2020 data. This suggests that we need a longer period of time in the future to investigate and determine whether the number of MCSs in JJA in the Mei-Yu region is trending increasing in the long term.

The number of MCSs generated in JJA over the Mei-Yu region accounts for 52% of the

annual total, which is larger than the 38% over East Asia. This suggests a more pronounced seasonal cycle over the Mei-Yu region. The number of MCSs generated in JJA is the highest for any three-month season. Hence, in analysing the environments of MCSs in the Mei-Yu region, we only selected the data in JJA.

In the Mei-Yu region, the highest MCS numbers occurred in 2020 for both the entire year and the JJA period. Although the number of MCSs generated in JJA is not the lowest in 2004 with only 2 more MCSs than in 2017, the annual number of MCSs is the lowest in 2004. And the number of MCSs generated in JJA is much lower than the average. Hence, we selected data for 2004 and 2020 to compare and analyse the environments of MCSs over the Mei-Yu region.



**Figure 4-11** Time series of MCS generation over the Mei-Yu region from 2001 to 2020. (a) Number of MCSs generated in the whole year; (b) number of MCSs generated in JJA.

## 4.2.2 Comparison between 2004 and 2020

As we did in Section 4.1.2, we do the same here for a pair of years over the Mei-Yu region. Figure 4-12 shows monthly MCS generation over the Mei-Yu region in 2004 and 2020. The month with the highest number of MCSs generated in the Mei-Yu region in 2020 is July with 134, and the month with the lowest number is December with 11. The month with the highest number of MCSs generated in the Mei-Yu region in 2004 is June with 77, and the months with the lowest number are January and December both with only 6.

The number of MCSs generated in JJA in 2020 is 336, while the number in JJA in 2004 is 190, which means that the number of MCSs generated in JJA in 2020 in the Mei-Yu region has increased by 76.84% compared to 2004. Hence, the main reason for the anomalously low number of MCSs in the Mei-Yu region in 2004 is related to the anomalous drop in the number of MCSs generated in July 2004.

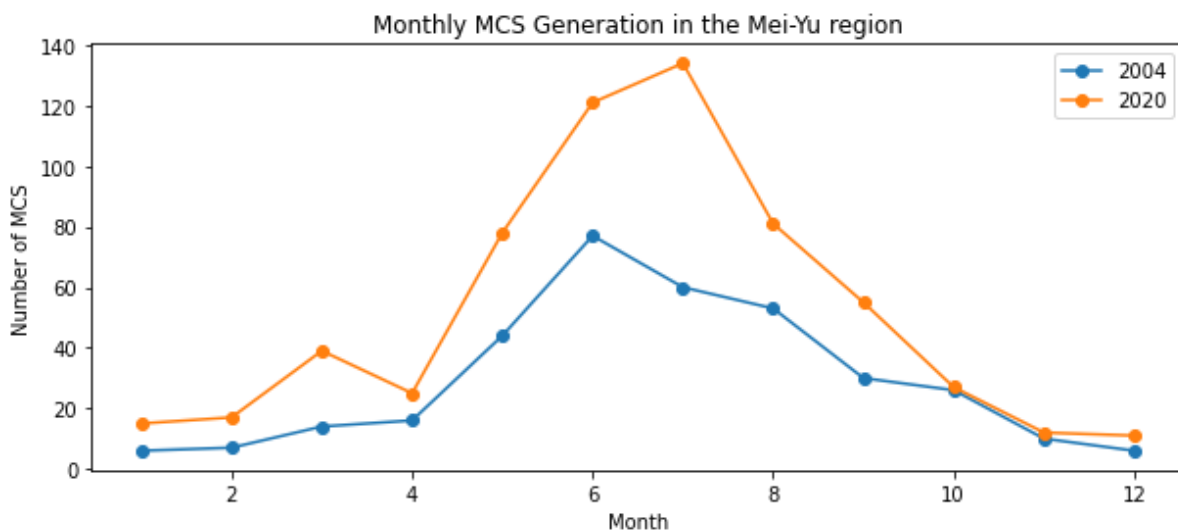


**Figure 4-12** Monthly MCS generation in the Mei-Yu region in 2004 and 2020.

Figure 4-13 shows the heat map differences of MCS numbers over the Mei-Yu region. Over the Mei-Yu region, the heat map difference of MCS numbers in JJA (Figure 4-13 b)

follows a very similar pattern to the annual heat map difference (Figure 4-13 a). Hence, it is sufficient to select only the environmental conditions in JJA for the analysis.

In spatial distribution, most regions, with the exception of parts of the Northwest, have more MCSs in 2020 than in 2004. The two regions with large differences in the number of MCSs are eastern China and the line from the Okinawa Islands to the four main islands of Japan. On the whole, the difference between the number of MCSs in 2020 and 2004 in the Mei-Yu region is highly substantial (Figure 4-13).

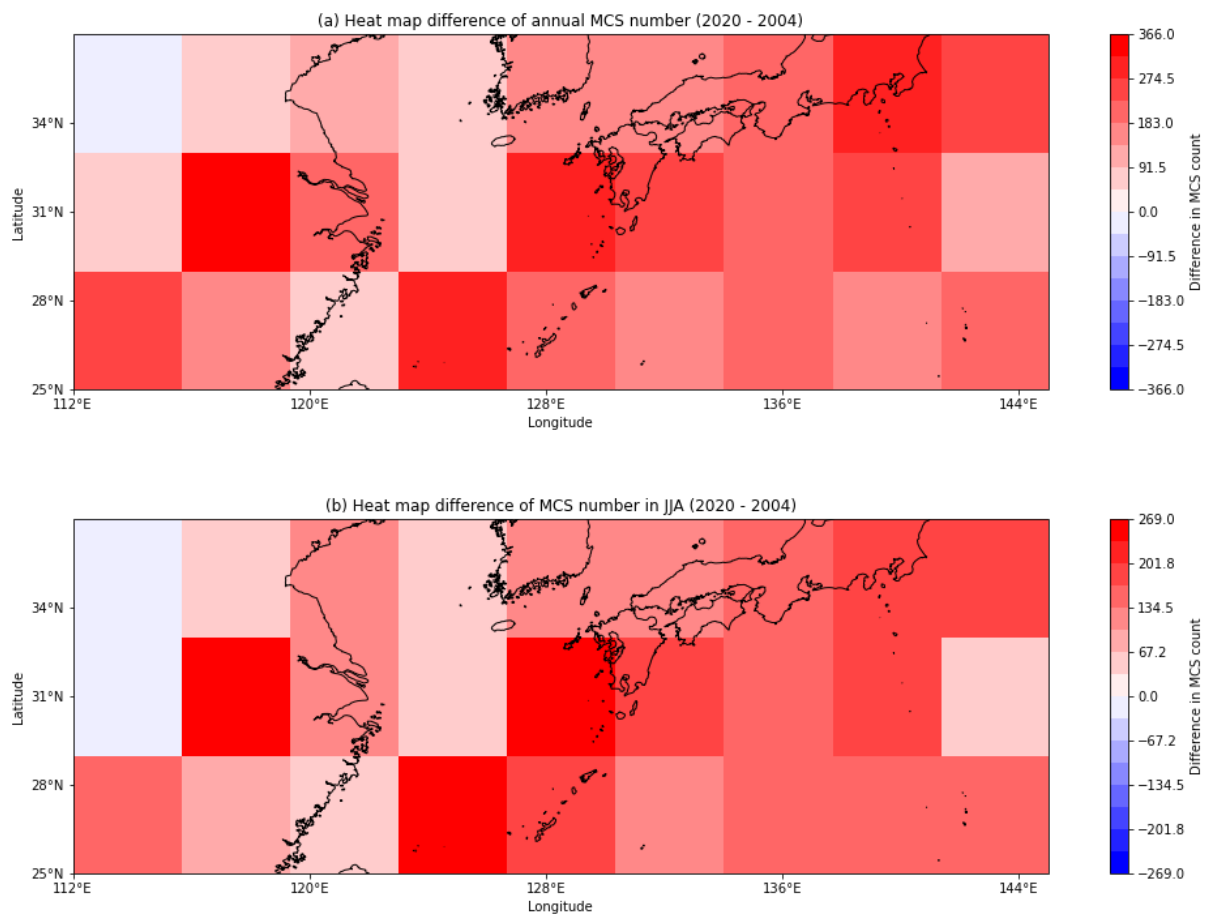


**Figure 4-13** Heat map differences of MCS numbers over the Mei-Yu region. (a) Heat map difference of annual MCS number for 2020 minus 2004; (b) heat map difference of MCS number in JJA for 2020 minus 2004.

### 4.2.3 Analysis of thermodynamic conditions

In the Mei-Yu region, CAPE in 2004 and 2020 shows a latitudinal variation over the ocean (Figure 4-14 a, c). TCWV does not vary substantially, but the region with lower latitude has generally higher TCWV than the region with higher latitude (Figure 4-14 b, d). The value of CAPE in 2020 is larger than in 2004 in the East China Sea, the Northwest Pacific Ocean, and the coastal region of the East China Sea, especially in the southern East China Sea ( $25^{\circ}\text{N}$ - $30^{\circ}\text{N}$ ,  $122^{\circ}\text{E}$ - $136^{\circ}\text{E}$ ), where the difference is substantial. The values of CAPE in 2020 are smaller than in 2004 over most of the land as well as in the Huanghai Sea, especially in the Huaihe River Basin in China ( $30^{\circ}\text{N}$ - $37^{\circ}\text{N}$ ,  $112^{\circ}\text{E}$ - $122^{\circ}\text{E}$ ), where the difference is substantial (Figure 4-14 e). The values of TCWV in 2020 are larger than those in 2004 in almost all parts of the Mei-Yu region, especially in the eastern part of China and the western part of the East China Sea ( $26^{\circ}\text{N}$ - $33^{\circ}\text{N}$ ,  $112^{\circ}\text{E}$ - $128^{\circ}\text{E}$ ), and their differences are substantial (Figure 4-14 f).

We compared the differences in MCS-initiation composite CAPE and the differences in MCS-initiation composite TCWV in the Mei-Yu region to the heat map differences of the number of MCSs, respectively (Figure 4-15).

Over the ocean in the southeastern part of the Mei-Yu region, CAPE in 2020 are larger than in 2004, while the number of MCSs in 2020 is also larger than in 2004 in this region (Figure 4-15 a). It appears that the pattern of CAPE differences and differences in the number of MCSs is similar in the maritime region. However, in most continental regions, such as most inland regions of China, the patterns of differences in CAPE and heat map differences of MCS number do not match. Hence, the pattern of differences in CAPE and differences in the number of MCSs does not seem to match overall.

Just as the number of MCSs in 2020 is greater than in 2004 in almost all parts of the Mei-Yu region, TCWV in 2020 is greater than in 2004 in almost all parts of this region (Figure 4-15 b). Although there are still some differences in the details of the spatial pattern, the pattern of differences in TCWV and the pattern of the heat map difference of MCS number match closely. Thus, as with the East Asia region, CAPE appears not to be a good predictor of the differences

between the two years, whereas TCWV performs much more strongly.

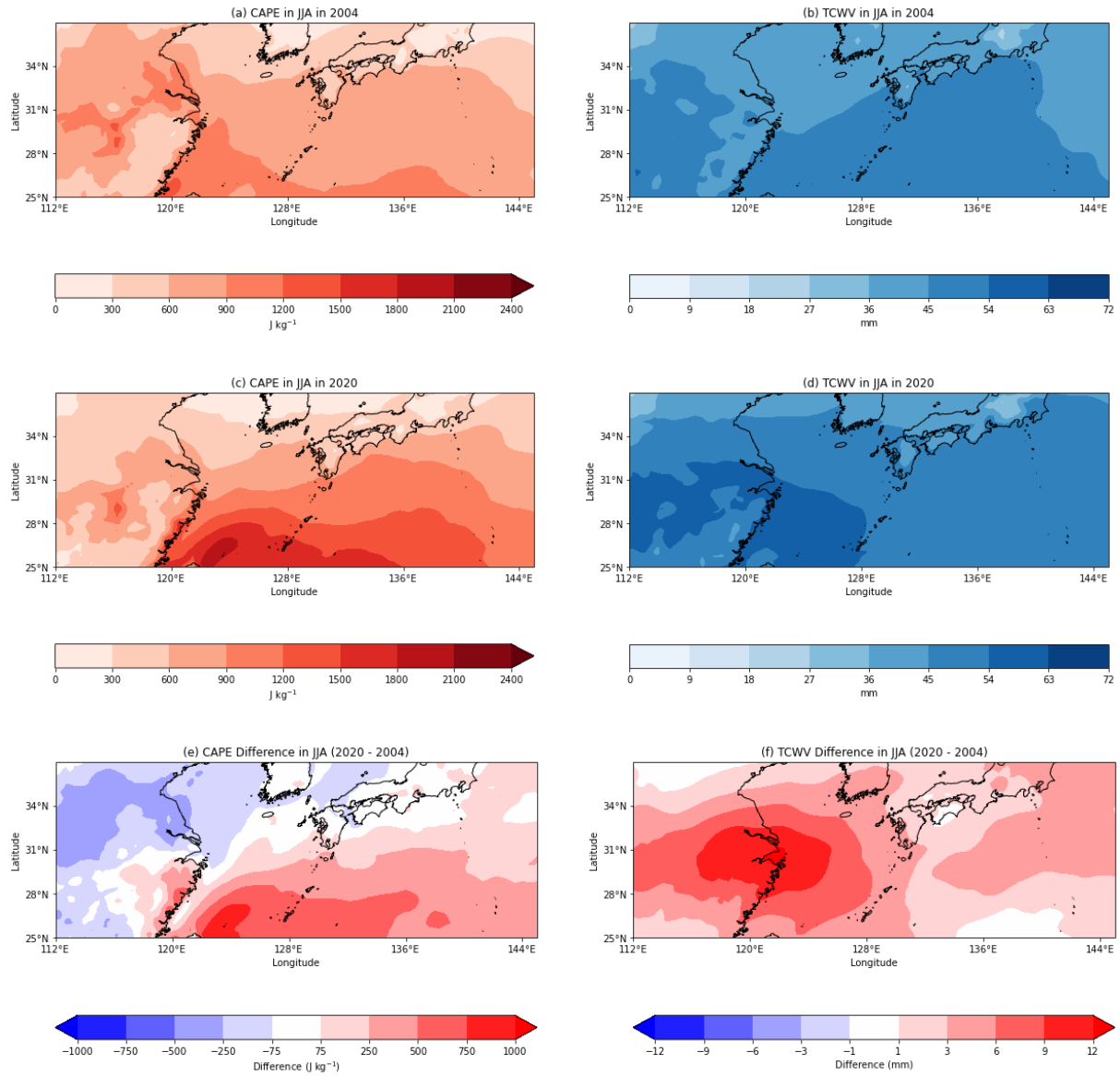


**Figure 4-14** Distribution of CAPE and TCWV at the times of MCS initiation over the Mei-Yu region in 2004 and 2020 and differences between the two years. (a) Distribution of CAPE over the Mei-Yu region in JJA in 2004; (b) distribution of TCWV over the Mei-Yu region in JJA in 2004; (c) distribution of CAPE over the Mei-Yu region in JJA in 2020; (d) distribution of TCWV over the Mei-Yu region in JJA in 2020; (e) distribution of CAPE difference between 2004 and 2020 (2020 - 2004) over the Mei-Yu region in JJA; (f) distribution of TCWV difference between 2004 and 2020 (2020 - 2004) over the Mei-Yu region in JJA.

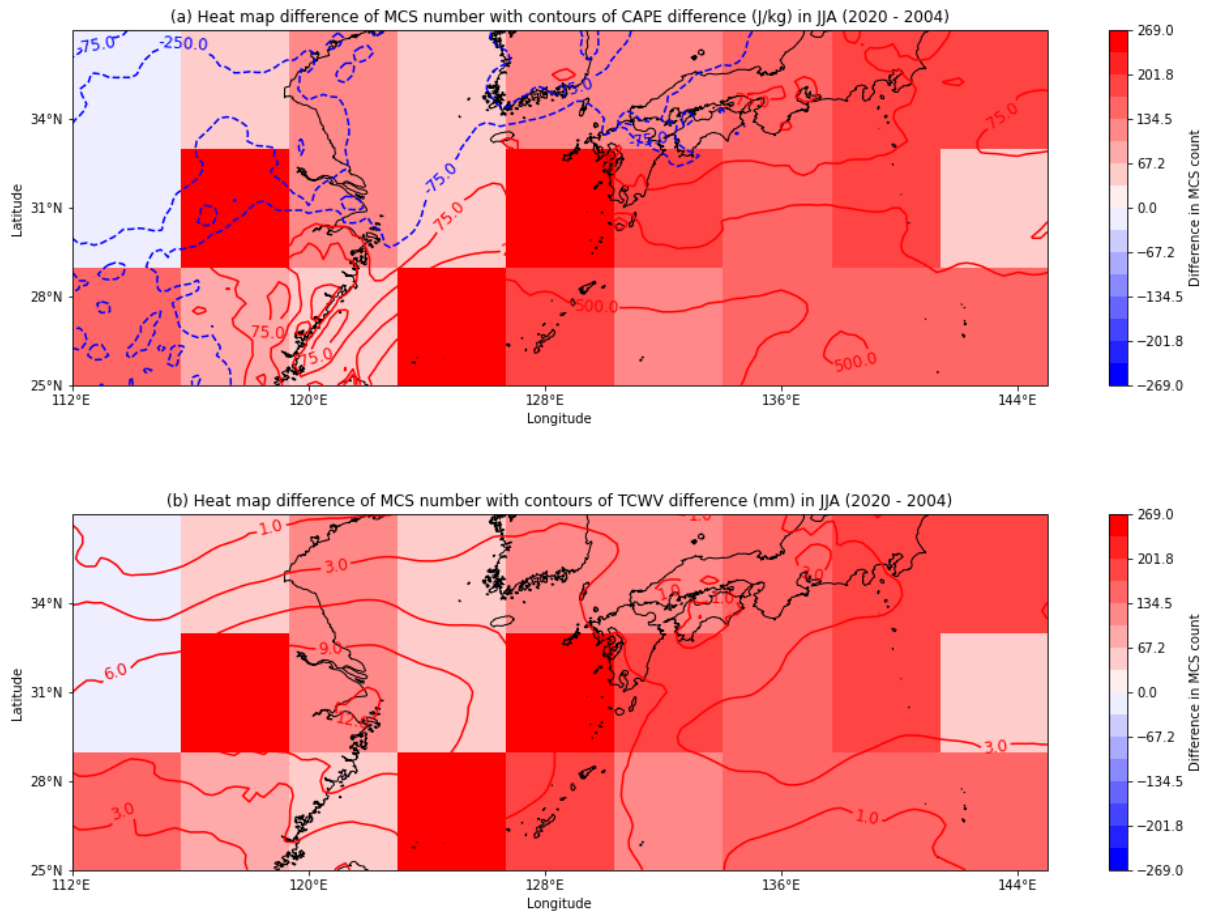


**Figure 4-15** Heat map differences of MCS number between 2004 and 2020 with contours of the CAPE and TCWV differences at the times of MCS initiation over the Mei-Yu region for both years. (a) The heat map with contours of the CAPE difference (2020 - 2004); (b) the heat map with contours of the TCWV difference (2020 - 2004).

#### 4.2.4 Analysis of dynamic conditions

After analysing the thermodynamic conditions in the Mei-Yu region, we proceeded to the dynamic conditions. VWS and VIMFD used here are composited on MCS initiation over the region. By comparison, shallow VWS is much stronger in 2020 than in 2004 over much of the Mei-Yu region (Figure 4-16 a). But, mid-level VWS in 2020 is much weaker than that in 2004 in the region along the west coast of the East China Sea (Figure 4-16 b). Combining the two intervals, deep-layer VWS in 2020 is still much stronger than in 2004 over much of the Mei-Yu region (Figure 4-16 c). As for VIMFD, although there is much more noise in the figure, it is still possible to identify that in much of the Mei-Yu region, VIMFD in 2020 is much lower than

in 2004, implying that there is more convergence in 2020 than in 2004 in these regions (Figure 4-16 d).

By comparing VWS differences at each of the three intervals with the heat map differences in the number of MCSs, the pattern of shallow VWS differences best matches the heat map differences (Figure 4-17 a, b, c). Mid-level VWS difference is the worst matched (Figure 4-17 b). Since deep-layer VWS is a combination of two other intervals, the pattern of deep-layer VWS also roughly matches the heat map difference of MCS number, it is not the best match (Figure 4-17 c). The pattern of VIMFD difference is also roughly matched to the heat map difference after ignoring the noisiness of this variable (Figure 4-17 d).

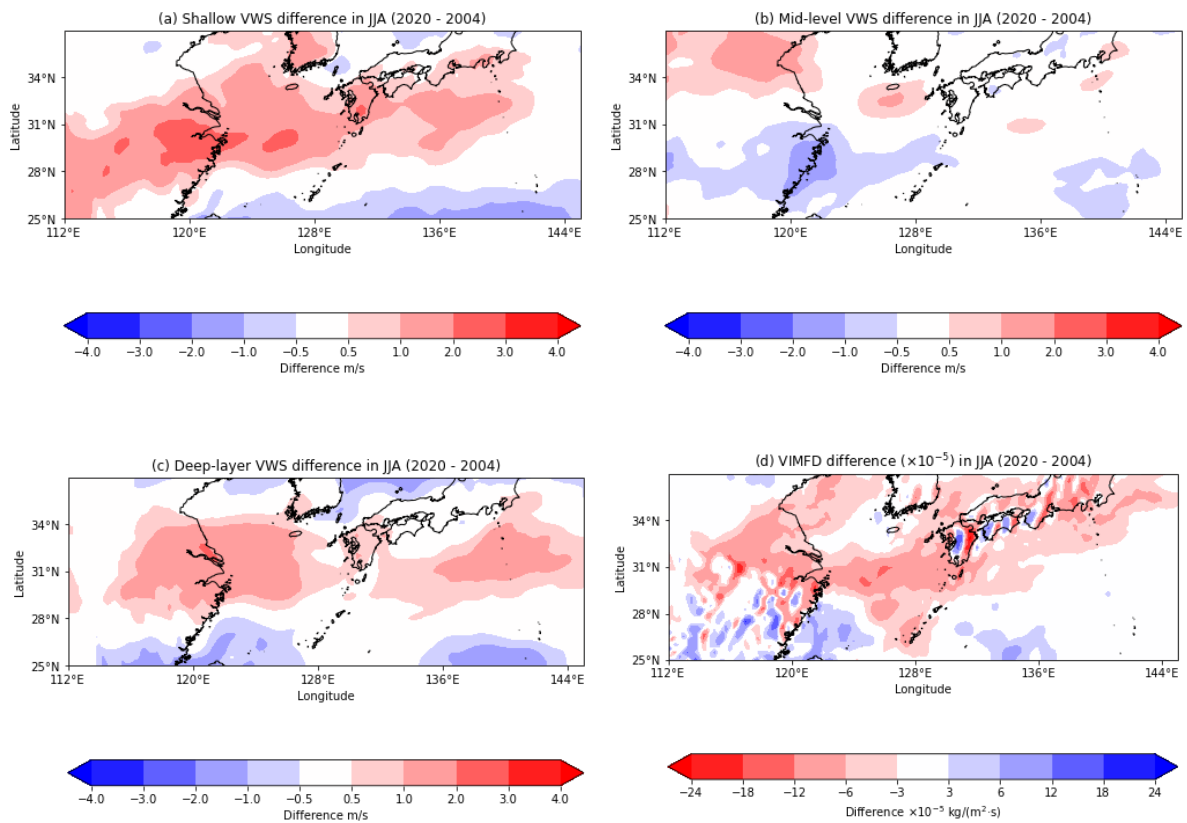


**Figure 4-16** Distribution of VWS difference and VIMFD difference at the times of MCS initiation over the Mei-Yu region in JJA between 2004 and 2020. (a) Distribution of VWS difference between surface and 800 hPa (2020 - 2004); (b) distribution of VWS difference between 800 hPa and 600 hPa (2020 - 2004); (c) distribution of VWS difference between surface and 600 hPa (2020 - 2004); (d) distribution of VIMFD difference between two years (2020 - 2004).

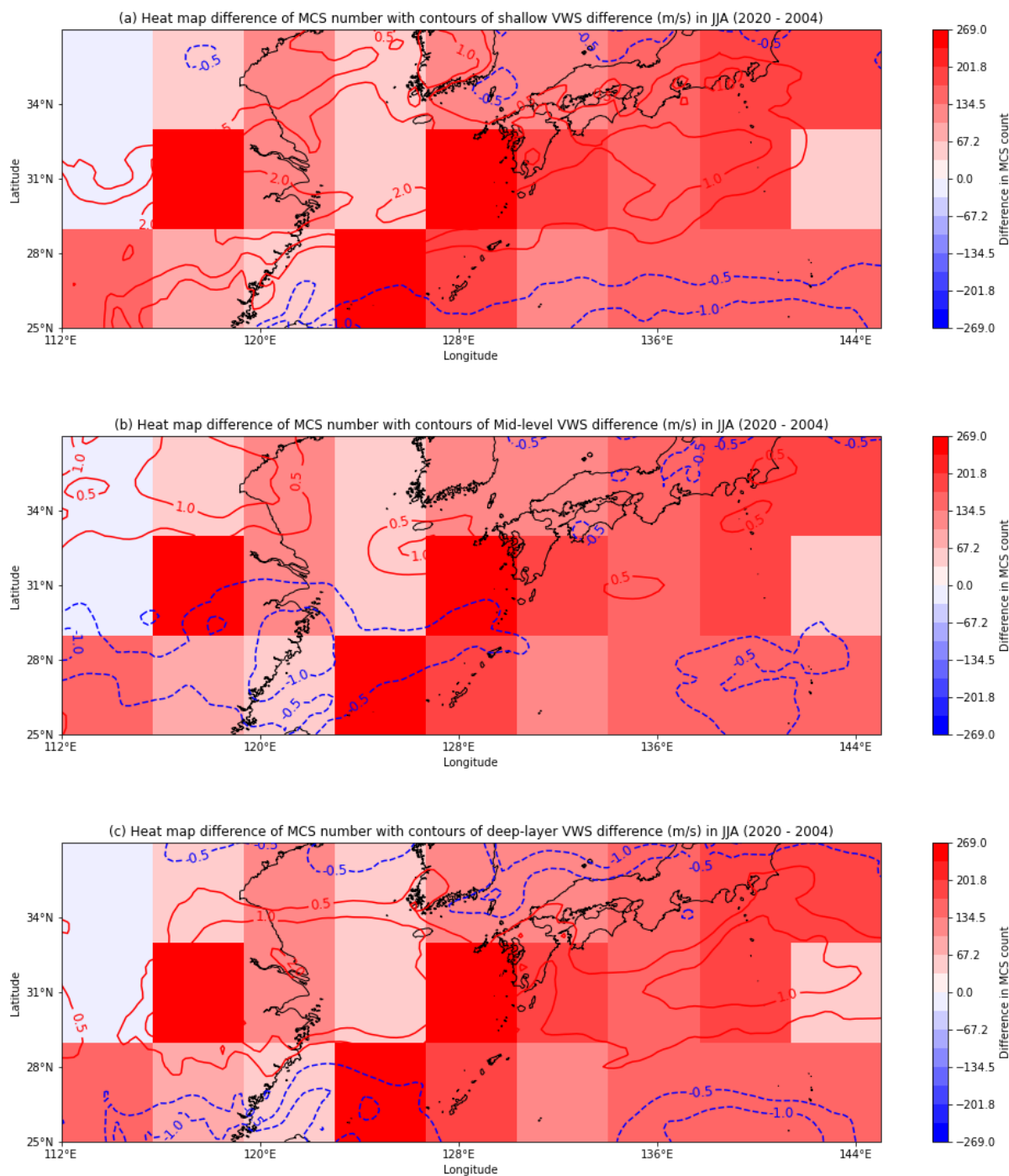


**Figure 4-17** Heat map differences in the number of MCSs between 2004 and 2020 with contours of the VWS and VIMFD differences at the times of MCS initiation over the Mei-Yu region for both years. (a) The heat map with contours of the VWS difference between surface and 800 hPa (2020 - 2004); (b) the heat map with contours of the VWS difference between 800 hPa and 600 hPa (2020 - 2004); (c) the heat map with contours of the VWS difference between surface and 600 hPa (2020 - 2004).

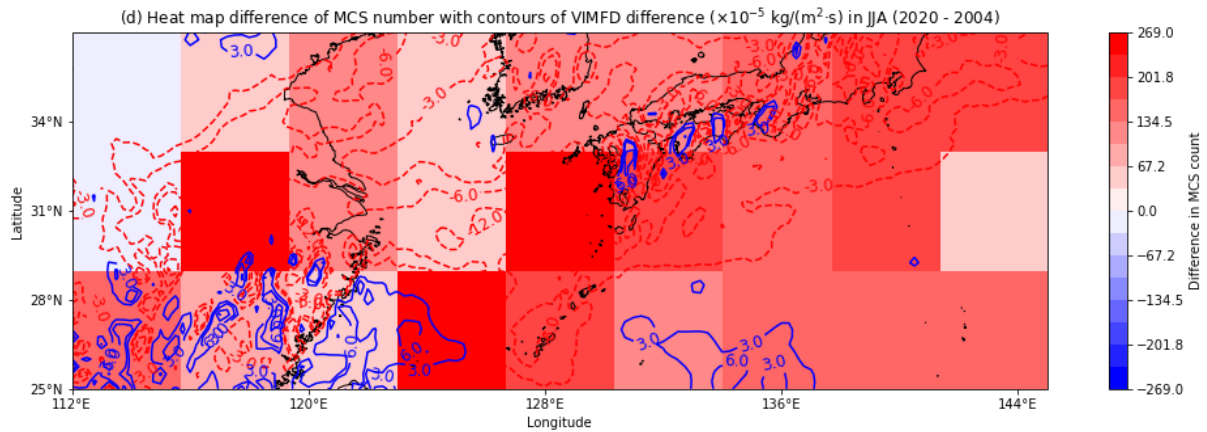


**Figure 4-17** Heat map differences in the number of MCSs between 2004 and 2020 with contours of the VWS and VIMFD differences at the times of MCS initiation over the Mei-Yu region for both years. (d) The heat map with contours of the VIMFD difference (2020 - 2004).

#### 4.2.5 Analysis of individual months

In Section 4.2.2, we found that there is a big difference in the number of MCSs generated in the month of July between the two years. In order to further investigate whether changes in environmental conditions made the number of MCSs generated in July 2020 in the Mei-Yu region much larger than in 2004, we plotted the differences in MCS-initiation composite environmental conditions between 2020 and 2004 in the Mei-Yu region in July (Figure 4-18). The patterns of TCWV, shallow VWS, deep-layer VWS, and VIMFD are all very similar, and their conditions in July are well suited for MCSs initiation (Figure 4-18 b, c, e, f). However, the CAPE difference has a wide range of negative values in the July pattern, especially over land (Figure 4-18 a). The pattern of mid-level VWS difference is also different from other environmental conditions (Figure 4-18 b). Comparing CAPE with mid-level VWS, two environmental conditions whose patterns are different from the others, we find that there seems to be a link between the two. The region of negative values for the CAPE difference corresponds well to the region of positive values for the mid-level VWS difference. Similarly, the region on land with positive values of the CAPE difference corresponds well with the region on land with negative values of the mid-level VWS difference.

Furthermore, we compared the spatial patterns of different environmental conditions in

July (Figure 4-18) with those in JJA (Figure 4-14 e, f, Figure 4-16). We found that their spatial patterns were consistent. This indicates that there is not much intra-seasonal variation of these environmental conditions in JJA.

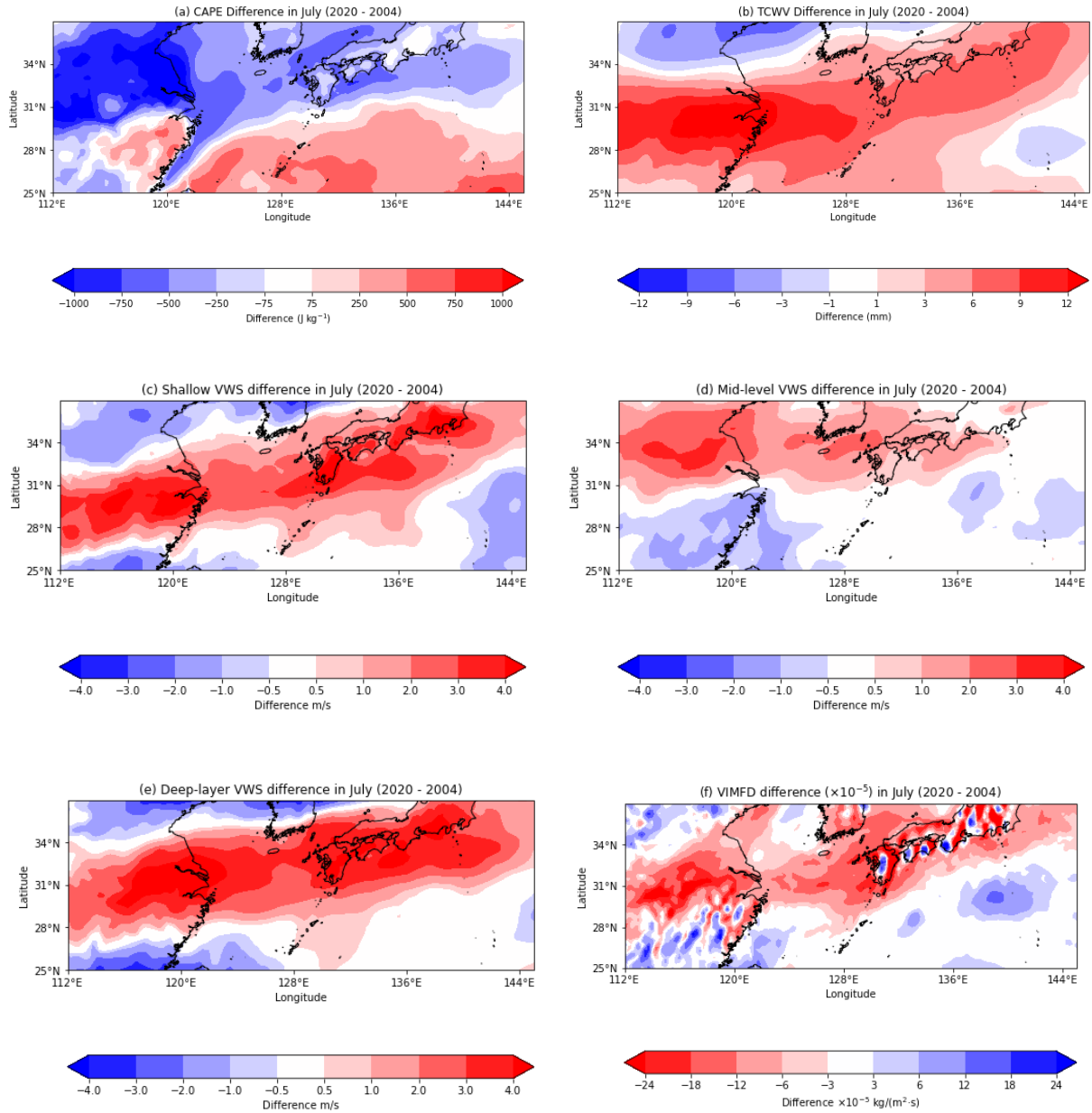


**Figure 4-18** Differences of MCS-initiation composite environmental conditions in July between 2004 and 2020 (2020 - 2004). (a) CAPE; (b) TCWV; (c) shallow VWS; (d) mid-level VWS; (e) deep-layer VWS; (f) VIMFD.

## 4.2.6 Correlation analysis

To statistically investigate the correlation of these MCS-initiation composite environmental conditions over the Mei-Yu region, we calculated the correlation coefficients between the number of MCSs and all MCS-initiation composite environmental conditions over the Mei-Yu region and plotted them as a correlation matrix (Figure 4-19). In terms of correlation coefficients between the number of MCSs and other environmental conditions, the largest is between CAPE and the number of MCSs, with a value of 0.44, which implies that the pattern of CAPE is more similar to that of the number of MCSs. This is followed by correlation coefficient between VIMFD and the number of MCSs and correlation coefficient between mid-level VWS and the number of MCSs, with values of -0.28 and -0.25, respectively. To our surprise, the correlation coefficient between TCWV and the number of MCSs is only 0.07 in the Mei-Yu region, which seems to be a big difference from our expected results in Section 4.2.3 and our results for the East Asia region as a whole in Section 4.1.6.

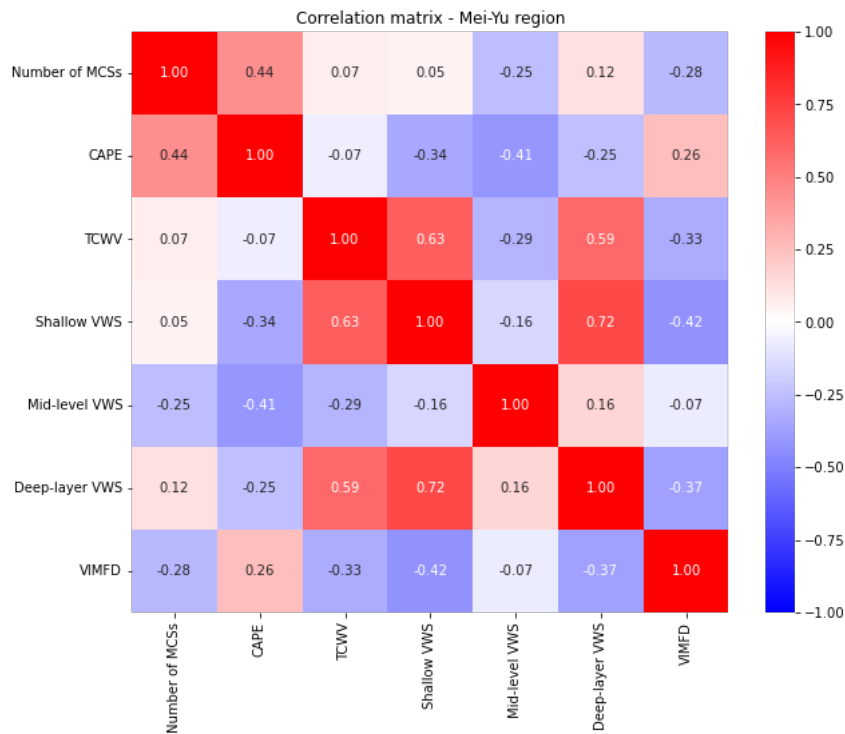


**Figure 4-19** Correlation matrix of the number of MCSs and various environmental conditions over the Mei-Yu region.

Between different MCS-initiation composite environmental conditions, mid-level VWS shows a weak association with shallow VWS and deep-layer VWS, with correlation coefficients of -0.16 and 0.16, respectively. TCWV is strongly associated with both shallow VWS and deep-layer VWS with correlation coefficients of 0.63 and 0.59, respectively. Similar spatial patterns do exist for TCWV, shallow VWS, and deep-layer VWS in Figure 4-18 (b, c, e). The possible reason for this is that the increase in all three environmental conditions is due to the same weather systems, the Mei-Yu fronts.

## 5 Discussion

### 5.1 MCS inter-annual and inter-monthly comparisons

In this study, we used a high-resolution ( $\sim 10$  km, 1 h) MCS tracking database (Feng et al. 2021) and ERA5 (Hersbach et al. 2020) to investigate the environment in which MCSs are generated over East Asia and the Mei-Yu region. We used the tracked trajectories of MCSs within East Asia ( $0^{\circ}$ - $55^{\circ}$ N,  $95^{\circ}$ E- $165^{\circ}$ E) and Mei-Yu region ( $25^{\circ}$ N- $37^{\circ}$ N,  $112^{\circ}$ E- $145^{\circ}$ E) for two decades (2001-2020) and compared the annual number of MCSs to the number of MCSs generated in JJA only. After comparison (Figure 4-1, Figure 4-11), we selected 2008 and 2015 to investigate the MCS initiation environments over East Asia and selected 2004 and 2020 to investigate the Mei-Yu region.

Yang et al. (2015) used data from the geostationary satellite Fengyun 2 series to investigate the number of MCSs in the region around China ( $18^{\circ}$ N- $55^{\circ}$ N,  $70^{\circ}$ E- $140^{\circ}$ E) from May to August 2005 to 2012 and found that the average number of MCSs generated during the eight years of the warm season was 1,087, and the highest number of MCSs was generated in 2010, followed by 2008. The geographic domain of their study falls between the regional domain of East Asia and the Mei-Yu region selected in this study, and the average number of MCSs also falls between the average number of MCSs in the two regions of this study. For the data on the number of MCSs in this study, if limited to the years 2005 to 2012, the year with the largest number of MCSs generated in JJA over East Asia is likewise 2010, followed by 2008 (Figure 4-1 b). Yang et al. (2015) also found that the number of MCSs generated peaked in July. The results of this study are also in line with this finding (Figure 4-2, Figure 4-12). This comparison demonstrates that the data on the number of MCSs in the two regions counted in the dataset used in this study are reliable.

MCSs in eastern China, which is included in the Mei-Yu region, show an obvious seasonal cycle (Li et al. 2020). In the current study, the number of MCSs generated in JJA over the Mei-Yu region as a proportion of the annual total, with a value of 52%, is greater than over East Asia, with a value of 38%. The difference in proportions is due to the strong seasonal cycle of

the number of MCSs over the Mei-Yu region.

## 5.2 MCS environments over East Asia

For the environmental conditions, we selected CAPE, TCWV, shallow VWS (between surface and 800 hPa), mid-level VWS (between 800 and 600 hPa), deep-layer VWS (between surface and 600 hPa), and VIMFD.

For convection initiation over East Asia, the presence of CAPE is a necessary condition, but that does not necessarily mean that more CAPE will initiate more convection (Chen et al. 2017). Sherwood (1999) analysed the environmental conditions for convective initiation in the tropical western Pacific by modeling and found that CAPE does not play an important role in convective initiation. They found that the threshold of CAPE required for probable convective initiation was around  $100\text{-}300 \text{ J}\cdot\text{kg}^{-1}$ , which was reached 86% of the time in the tropical western Pacific, and that higher CAPE above the threshold did not affect the probability of convective initiation. The low correlation between the MCS-initiation composite CAPE and the number of MCSs in this study may be explained by this. That is, the magnitude of CAPE has a relatively weak effect on the probability of MCS initiation when environmental conditions reach above the threshold where CAPE is sufficient for MCS initiation.

Past studies have shown that MCS initiation in the tropics is closely related to increased water vapour in the troposphere (Holloway and Neelin 2009). In this study, we also found a relatively close relationship between the MCS-initiation composite TCWV and MCS initiation over East Asia (Figure 4-9). However, by dividing East Asia into two regions ( $0^{\circ}\text{-}28^{\circ}\text{N}$  and  $28^{\circ}\text{N}\text{-}55^{\circ}\text{N}$ ), we found that the relationship between the MCS-initiation composite TCWV and MCS initiation is very strong in the region of low latitudes at  $0^{\circ}\text{-}28^{\circ}\text{N}$  (Figure 4-10 a), but there is not much relationship at  $28^{\circ}\text{N}\text{-}55^{\circ}\text{N}$  (Figure 4-10 b). Thus, in the low-latitude tropics, we find a conclusion consistent with Holloway and Neelin (2009), that TCWV plays an important role in MCS initiation in the tropics. In contrast, this study extends its analysis to the mid-latitude region, revealing that MCS initiation in the mid-latitude region is not strongly affected

by TCWV.

VWS has been proved by several studies to have a role in MCS initiation and development, especially in mid-latitudes (Grant et al. 2020; Coniglio and Stensrud 2001). In this study, the relationship between the MCS-initiation composite VWS and MCS initiation is not obvious for the whole of East Asia. However, after we divided East Asia into  $0^{\circ}$ - $28^{\circ}$ N and  $28^{\circ}$ N- $55^{\circ}$ N, the MCS-initiation composite VWS showed a negative correlation with the number of MCSs at  $0^{\circ}$ - $28^{\circ}$ N, and a certain positive correlation with the number of MCSs at  $28^{\circ}$ - $55^{\circ}$ N. Among the three intervals considered, the relationship between the shallow VWS and the number of MCSs is the strongest. Thus, the role of VWS in MCS initiation is again validated in the mid-latitudes of  $28^{\circ}$ N- $55^{\circ}$ N. Grant et al. (2018) found that in tropical oceanic regions, the strengthening of the cold pool by shear reduces the speed of updrafts and thus inhibits the formation of convection. VWS can enhance the formation and development of cold pools (Schumacher and Rasmussen 2020). This may explain the negative correlation between VWS and MCS initiation at  $0^{\circ}$ - $28^{\circ}$ N found in this study. That is, in the tropical western Pacific at  $0^{\circ}$ - $28^{\circ}$ N, stronger VWS produces stronger cold pools, which suppresses the updraft speed and ultimately the MCS initiation.

Vertically integrated moisture flux convergence produces a moist environment that promotes MCS initiation (Tsuji et al. 2021). In this study, the MCS-initiation composite VIMFD showed a strong negative correlation with MCS initiation. More negative VIMFD represents stronger vertically integrated moisture flux convergence. Thus, we can say that vertically integrated moisture flux convergence shows a strong positive correlation with MCS initiation, which is also consistent with the conclusion of Tsuji et al. (2021). This relationship holds in the tropics and at higher latitudes.

Here, we have selected 2008 and 2015 for comparison. In 2007/2008, La Niña occurred (Hoell et al. 2014). 2015/2016 was the first extreme El Niño event of the century (Santoso et al. 2017). As in Figure 2-5, Liu et al. (2019) compared the proportion of MCSs to precipitation systems in El Niño years with La Niña years, indicating that the proportions of MCS in the South China Sea and around the Philippines are lower in El Niño years than in La Niña years,

whereas the proportions of MCS in eastern China are higher in El Niño years than in La Niña years. In this study, the number of MCSs in the South China Sea and around the Philippines in 2015, which is an extreme El Niño year, is less than that in 2008, which is a La Niña year, and the number of MCSs in eastern China in 2015 is more than that in 2008 (Figure 4-3). Thus, the difference in the number of MCSs between the two years is consistent with the general expectations for the difference between El Niño and La Niña event years. Hence ENSO played an important role in these two years.

### **5.3 MCS environments over the Mei-Yu region**

The record-breaking Mei-Yu rains occurred in the summer of 2020 (Volonté et al. 2021). The reasons for this have been analysed by Ding et al. (2021). They suggested that one of the major reasons is the enhancement of the low-level southwesterly jet. Additionally, the MJO was persistently active in the Indian Ocean for 59 days from June to July 2020, transporting abundant water vapour to East Asia (Zhang et al. 2021). In this study, we found that the MCS-initiation composite TCWV in the Mei-Yu region was much higher overall in 2020 than in 2004 (Figure 4-14 f). This may be related to the enhanced low-level southwesterly jet and the anomalous persistent MJO in the Indian Ocean. Another important reason found by Ding et al. (2021) was that the convergence zone formed by the constantly moving southward cold air masses and warm moist air masses from the India Ocean caused the long-lasting heavy precipitation. In this study, we found that the MCS-initiation composite VIMFD in 2020 in the Mei-Yu region is much more negative than that in 2004 in overall terms (Figure 4-16 d). This means that there is more vertically integrated moisture flux convergence in 2020 than in 2004 in the Mei-Yu region. The enhancement of convergence in 2020 also verifies the analysis from Ding et al. (2021). In addition to that, in Section 5.2, we analysed the important role of VWS for MCS initiation in mid-latitudes. In this study, we similarly found an overall larger MCS-initiation composite shallow VWS in 2020 than in 2004 (Figure 4-16 a). This verifies the previous analysis about VWS in Section 5.2 once again.

## 5.4 Limitations and future work

In this study, two years with high and low generation numbers of MCSs in JJA over East Asia and the Mei-Yu region were selected to compare and analyse the MCS-initiation composite environmental conditions. For East Asia, we selected 2008 and 2015 for comparison, and for the Mei-Yu region, we selected 2004 and 2020 for comparison. It may not be sufficient to select only one pair of years of MCS-initiation composite environmental conditions. We need data from more years for further analysis to obtain more general conclusions. Meanwhile, we also need to exclude some special conditions from interfering with the analyses. Finally, this study only investigated CAPE, TCWV, VWS and VIMFD. There are many other environmental conditions that are associated with MCS initiation that we could further analyse. For example, we found that TCWV is important in the tropics, and it could be interesting to see if there are different types of relationship for the water vapour content at different levels of the atmosphere.

As discussed in Section 5.3, MCSs in the Mei-Yu region have also been associated with environmental conditions in the Indian Ocean. The analyses of environmental conditions in this study are limited to the corresponding regions. This may miss some of the relationships or teleconnections between MCS initiation and environmental conditions in neighbouring regions such as the Indian Ocean.

## 6 Conclusion

This study investigated MCS environments over East Asia and the Mei-Yu region, mainly by comparing and analysing the MCS-initiation composite environmental conditions in the two years when MCSs were generated in their highest and lowest numbers.

During the two decades from 2001 to 2020, East Asia ( $0^{\circ}$ - $55^{\circ}$ N,  $95^{\circ}$ E- $165^{\circ}$ E) experiences 5,951 MCSs annually on average, and the number of MCSs is generally stable over time. The Mei-Yu region ( $25^{\circ}$ N- $37^{\circ}$ N,  $112^{\circ}$ E- $145^{\circ}$ E) experiences about 467 MCSs annually on average, and the number of MCSs shows a long-term upward trend.

In East Asia, the MCS-initiation composite TCWV has a strong positive correlation with the number of MCSs, and thus TCWV is one of the important factors influencing MCS initiation. The strong negative correlation between MCS-initiation composite VIMFD and the number of MCSs implies a strong positive correlation between vertically integrated moisture flux convergence and the number of MCSs. Thus, moisture convergence plays an important role in MCS initiation. Furthermore, this relationship holds at tropical latitudes and mid-latitudes. VWS has different effects on MCS initiation at different latitudes. At tropical latitudes, VWS inhibits MCS initiation, whereas at mid-latitudes, VWS, especially the shallow VWS, promotes MCS initiation. There is not a strong relationship between CAPE and MCS initiation.

In the Mei-Yu region, one of the main contributors to the larger number of MCS in 2020 than in 2004 is TCWV. The MCS-initiation composite VIMFD in 2020 is also overall smaller compared to 2004, implying that there is more moisture convergence in 2020, and thus moisture convergence is also important for MCS initiation. Furthermore, the MCS-initiation composite shallow VWS in 2020 is also much stronger than in 2004.

In the future, the topics of this study could be further investigated and analysed. It would be a good idea to use more years of data on the MCS-initiation composite environmental conditions to draw more general conclusions. We can also further investigate whether there is some trend in the environmental conditions over time during the last two decades. In addition

to the environmental conditions investigated in this study, we can also investigate other environmental conditions as well as the impact of large-scale drivers on MCS initiation and trends over the last two decades. For the Mei-Yu region, we can further investigate some environmental conditions in relevant adjacent regions, such as the Indian Ocean.

## References

- Allen, M. R., and W. J. Ingram, 2002: Constraints on future changes in climate and the hydrologic cycle. *Nature*, **419**, 224–232.
- Bretherton, C. S., M. E. Peters, and L. E. Back, 2004: Relationships between Water Vapor Path and Precipitation over the Tropical Oceans. *Journal of Climate*, **17**, 1517–1528.
- Charney, J. G., and A. Eliassen, 1964: On the Growth of the Hurricane Depression. *J Atmos Sci*, **21**, 68–75.
- Chen, B., C. Liu, and B. E. Mapes, 2017: Relationships between large precipitating systems and atmospheric factors at a grid scale. *J Atmos Sci*, **74**, 531–552.
- Chen, Q., J. Fan, S. Hagos, W. I. Gustafson, and L. K. Berg, 2015: Roles of wind shear at different vertical levels: Cloud system organization and properties. *J Geophys Res*, **120**, 6511–6574.
- Cheng, Y. M., J. Dias, G. Kiladis, Z. Feng, and L. R. Leung, 2023: Mesoscale Convective Systems Modulated by Convectively Coupled Equatorial Waves. *Geophys Res Lett*, **50**.
- Coniglio, M. C., and D. J. Stensrud, 2001: Simulation of a Progressive Derecho Using Composite Initial Conditions. *Mon Weather Rev*, **129**, 1593–1616.
- , ———, and L. J. Wicker, 2006: Effects of Upper-Level Shear on the Structure and Maintenance of Strong Quasi-Linear Mesoscale Convective Systems. *Journal of the Atmospheric Sciences*, **63**, 1231–1252.
- Ding, Y., and J. C. L. Chan, 2005: The East Asian summer monsoon: An overview. *Meteorology and Atmospheric Physics*, **89**, 117–142.
- , Y. Liu, and Z. Z. Hu, 2021: The Record-breaking Mei-yu in 2020 and Associated Atmospheric Circulation and Tropical SST Anomalies. *Adv Atmos Sci*, **38**, 1980–1993.
- Emanuel, K. A., J. David Neelin, and C. S. Bretherton, 1994: On large-scale circulations in convecting atmospheres. *Quarterly Journal of the Royal Meteorological Society*, **120**, 1111–1143.
- Feng, Z., L. R. Leung, S. Hagos, R. A. Houze, C. D. Burleyson, and K. Balaguru, 2016: More frequent intense and long-lived storms dominate the springtime trend in central US rainfall. *Nat Commun*, **7**.
- , R. A. Houze, L. R. Leung, F. Song, J. C. Hardin, J. Wang, W. I. Gustafson, and C. R. Homeyer, 2019: Spatiotemporal Characteristics and Large-Scale Environments of Mesoscale Convective Systems East of the Rocky Mountains. *J Clim*, **32**, 7303–7328.
- , and Coauthors, 2021: A Global High-Resolution Mesoscale Convective System Database

- Using Satellite-Derived Cloud Tops, Surface Precipitation, and Tracking. *Journal of Geophysical Research: Atmospheres*, **126**.
- Fu, S. M., Z. Mai, J. H. Sun, W. L. Li, Y. Ding, and Y. Q. Wang, 2019: Impacts of convective activity over the tibetan plateau on plateau vortex, southwest vortex, and downstream precipitation. *J Atmos Sci*, **76**, 3803–3830.
- Galarneau, T. J., X. Zeng, R. D. Dixon, A. Ouyed, H. Su, and W. Cui, 2023: Tropical mesoscale convective system formation environments. *Atmospheric Science Letters*, **24**.
- Geerts, B., and Coauthors, 2017: The 2015 plains elevated convection at night field project. *Bull Am Meteorol Soc*, **98**, 767–786.
- Grant, L. D., T. P. Lane, and S. C. van den Heever, 2018: The role of cold pools in tropical oceanic convective systems. *J Atmos Sci*, **75**, 2615–2634.
- , M. W. Moncrieff, T. P. Lane, and S. C. van den Heever, 2020: Shear-Parallel Tropical Convective Systems: Importance of Cold Pools and Wind Shear. *Geophys Res Lett*, **47**.
- Guan, P., G. Chen, W. Zeng, and Q. Liu, 2020: Corridors of mei-yu-season rainfall over Eastern China. *J Clim*, **33**, 2603–2626.
- Haberlie, A. M., and W. S. Ashley, 2019: A radar-based climatology of mesoscale convective systems in the United States. *J Clim*, **32**, 1591–1606.
- Hart, N. C. G., R. Washington, and R. I. Maidment, 2019: Deep Convection over Africa: Annual Cycle, ENSO, and Trends in the Hotspots. *J Clim*, **32**, 8791–8811.
- Hersbach, H., and Coauthors, 2020: The ERA5 global reanalysis. *QUARTERLY JOURNAL OF THE ROYAL METEOROLOGICAL SOCIETY*, **146**, 1999–2049.
- Higgins, R. W., Y. Yao, E. S. Yarosh, J. E. Janowiak, and K. C. Mo, 1997: Influence of the Great Plains Low-Level Jet on Summertime Precipitation and Moisture Transport over the Central United States. *J Clim*, **10**, 481–507.
- Hoell, A., C. Funk, and M. Barlow, 2014: The regional forcing of Northern hemisphere drought during recent warm tropical west Pacific Ocean La Niña events. *Clim Dyn*, **42**, 3289–3311.
- Holloway, C. E., and D. J. Neelin, 2009: Moisture vertical structure, column water vapor, and tropical deep convection. *J Atmos Sci*, **66**, 1665–1683.
- , and J. D. Neelin, 2010: Temporal relations of column water vapor and tropical precipitation. *J Atmos Sci*, **67**, 1091–1105.
- Houze, R. A., 2004: Mesoscale convective systems. *Reviews of Geophysics*, **42**, 1–43.
- , 2018: 100 Years of Research on Mesoscale Convective Systems. *Meteorological Monographs*, **59**, 17.1-17.54.
- Houze, R. A., Jr., Rutledge S. A., Biggerstaff M. I., and Smull B. F., 1989: Interpretation of

- Doppler Weather Radar Displays of Midlatitude Mesoscale Convective Systems. *Bulletin American Meteorological Society*, **70**, 608–619.
- Hu, H., Z. Feng, and L.-Y. R. Leung, 2021: Linking Flood Frequency With Mesoscale Convective Systems in the US. *Geophys Res Lett*, **48**.
- Huffman, G. J., E. F. Stocker, D. T. Bolvin, E. J. Nelkin, and J. Tan, 2019: GPM IMERG Final Precipitation L3 Half Hourly 0.1 degree x 0.1 degree V06. Retrieved from Greenbelt, MD: Goddard Earth Sciences Data and Information Services Center (GES DISC),.
- Johns, R. H., and W. D. Hirt, 1987: Derechos: Widespread Convectively Induced Windstorms. *Weather Forecast*, **2**, 32–49.
- , and C. A. III. Doswell, 1992: Severe Local Storms Forecasting. *Weather Forecast*, **7**, 588–612.
- Kahraman, A., E. J. Kendon, S. C. Chan, and H. J. Fowler, 2021: Quasi-Stationary Intense Rainstorms Spread Across Europe Under Climate Change. *Geophys Res Lett*, **48**.
- Kiladis, G. N., M. C. Wheeler, P. T. Haertel, K. H. Straub, and P. E. Roundy, 2009: Convectively coupled equatorial waves. *Reviews of Geophysics*, **47**.
- Kummerow, C., W. Barnes, T. Kozu, J. Shiue, and J. Simpson, 1998: The Tropical Rainfall Measuring Mission (TRMM) sensor package. *J Atmos Ocean Technol*, **15**, 809–817.
- Laing, A. G., and J. Michael Fritsch, 1997: The global population of mesoscale convective complexes. *Quarterly Journal of the Royal Meteorological Society*, **123**, 389–405.
- Li, P., C. Moseley, A. F. Prein, H. Chen, J. Li, K. Furtado, and T. Zhub, 2020: Mesoscale convective system precipitation characteristics over East Asia. Part I: Regional differences and seasonal variations. *J Clim*, **33**, 9271–9286.
- Li, Y., and R. E. Carbone, 2012: Excitation of rainfall over the tropical western pacific. *J Atmos Sci*, **69**, 2983–2994.
- Liu, N., C. Liu, and T. Lavigne, 2019: The variation of the intensity, height, and size of precipitation systems with El Niño-Southern oscillation in the tropics and subtropics. *J Clim*, **32**, 4281–4297.
- Maddox, R. A., 1980: Mesoscale Convective Complexes. *Bulletin American Meteorological Society*, **61**, 1374–1400.
- Morel, C., and S. Senesi, 2002: A climatology of mesoscale convective systems over Europe using satellite infrared imagery. II: Characteristics of European mesoscale convective systems. *Quarterly Journal of the Royal Meteorological Society*, **128**, 1973–1995.
- Nakamura, Y., and Y. N. Takayabu, 2022a: Convective Couplings with Equatorial Rossby Waves and Equatorial Kelvin Waves. Part I: Coupled Wave Structures. *J Atmos Sci*, **79**, 247–262.

- , and ——, 2022b: Convective Couplings with Equatorial Rossby Waves and Equatorial Kelvin Waves. Part II: Coupled Precipitation Characteristics. *J Atmos Sci*, **79**, 2919–2933.
- Nesbitt, S. W. ;, and E. J. Zipser, 2003: The diurnal cycle of rainfall and convective intensity according to three years of TRMM measurements. *J Clim*, **16**, 1456–1475.
- Nesbitt, S. W., R. Cifelli, and S. A. Rutledge, 2006: Storm Morphology and Rainfall Characteristics of TRMM Precipitation Features. *Mon Weather Rev*, **134**, 2702–2721.
- Parker, M. D., and R. H. Johnson, 2000: Organizational Modes of Midlatitude Mesoscale Convective Systems. *Mon Weather Rev*, **128**, 3413–3436.
- Prein, A. F., C. Liu, K. Ikeda, S. B. Trier, R. M. Rasmussen, G. J. Holland, and M. P. Clark, 2017: Increased rainfall volume from future convective storms in the US. *Nat Clim Chang*, **7**, 880–884.
- Rasmussen, K. L., and R. A. Houze, 2012: A flash-flooding storm at the steep edge of high terrain. *Bull Am Meteorol Soc*, **93**, 1713–1724.
- Raymond, D., Ž. Fuchs, S. Gjorgjievska, and S. Sessions, 2015: Balanced dynamics and convection in the tropical troposphere. *J Adv Model Earth Syst*, **7**, 1093–1116.
- Raymond, D. J., and M. J. Herman, 2011: Convective quasi-equilibrium reconsidered. *J Adv Model Earth Syst*, **3**.
- Raymond, D. J., and Fuchs-Stone, 2021: Emergent Properties of Convection in OTREC and PREDICT. *Journal of Geophysical Research: Atmospheres*, **126**.
- Sampe, T., and S. P. Xie, 2010: Large-scale dynamics of the meiyu-baiu rainband: Environmental forcing by the westerly jet. *J Clim*, **23**, 113–134.
- Santoso, A., M. J. Mcphaden, and W. Cai, 2017: The Defining Characteristics of ENSO Extremes and the Strong 2015/2016 El Niño. *Reviews of Geophysics*, **55**, 1079–1129.
- Schultz, D. M., P. N. Schumacher, and C. A. Doswell Iii, 2000: The Intricacies of Instabilities. *Monthly Weather Review*, **128**, 4143–4148.
- Schumacher, R. S., and K. L. Rasmussen, 2020: The formation, character and changing nature of mesoscale convective systems. *Nat Rev Earth Environ*, **1**, 300–314.
- Sherwood, S. C., 1999: Convective Precursors and Predictability in the Tropical Western Pacific. *Mon Weather Rev*, **127**, 2977–2991.
- Sherwood, S. C., P. Minnis, and M. McGill, 2004: Deep convective cloud-top heights and their thermodynamic control during CRYSTAL-FACE. *Journal of Geophysical Research D: Atmospheres*, **109**.
- Simpson, J., R. F. Adler, and G. R. North, 1988: A Proposed Tropical Rainfall Measuring Mission (TRMM) Satellites. *Bull Am Meteorol Soc*, **69**, 278–295.

- Stevenson, S. N., and R. S. Schumacher, 2014: A -10-Year survey of extreme rainfall events in the central and eastern United States using gridded multisensor precipitation analyses. *Mon Weather Rev*, **142**, 3147–3162.
- Tan, J., G. J. Huffman, D. T. Bolvin, and E. J. Nelkin, 2019: IMERG V06: Changes to the Morphing Algorithm. *J Atmos Ocean Technol*, **36**, 2471–2482, <https://doi.org/10.1175/JTECH-D-19>.
- Taylor, C. M., and Coauthors, 2017: Frequency of extreme Sahelian storms tripled since 1982 in satellite observations. *Nature*, **544**, 475–478.
- Tomassini, L., 2021: The interaction between moist convection and the atmospheric circulation in the tropics. *Bull Am Meteorol Soc*, **101**, E1378–E1396.
- Trier, S. B., C. A. Davis, D. A. Ahijevych, and K. W. Manning, 2014: Use of the parcel buoyancy minimum (Bmin) to diagnose simulated thermodynamic destabilization. Part II: Composite analysis of mature MCS environments. *Mon Weather Rev*, **142**, 967–990.
- Tsuji, H., Y. N. Takayabu, R. Shibuya, H. Kamahori, and C. Yokoyama, 2021: The Role of Free-Tropospheric Moisture Convergence for Summertime Heavy Rainfall in Western Japan. *Geophys Res Lett*, **48**.
- Volonté, A., M. Muetzelfeldt, R. Schiemann, A. G. Turner, and N. Klingaman, 2021: Magnitude, Scale, and Dynamics of the 2020 Mei-yu Rains and Floods over China. *Adv Atmos Sci*, **38**, 2082–2096.
- , A. G. Turner, R. Schiemann, P. L. Vidale, and N. P. Klingaman, 2022: Characterising the interaction of tropical and extratropical air masses controlling East Asian summer monsoon progression using a novel frontal detection approach. *Weather and Climate Dynamics*, **3**, 575–599.
- Weisman, M. L., and C. A. Davis, 1998: Mechanisms for the Generation of Mesoscale Vortices within Quasi-Linear Convective Systems. *J Atmos Sci*, **55**, 2603–2622.
- Yang, R., Y. Zhang, J. Sun, S. Fu, and J. Li, 2019: The characteristics and classification of eastward-propagating mesoscale convective systems generated over the second-step terrain in the Yangtze River Valley. *Atmospheric Science Letters*, **20**.
- , ———, ———, and J. Li, 2020: The comparison of statistical features and synoptic circulations between the eastward-propagating and quasi-stationary MCSs during the warm season around the second-step terrain along the middle reaches of the Yangtze River. *Sci China Earth Sci*, **63**, 1209–1222.
- Yang, X., J. Fei, X. Huang, X. Cheng, L. M. V. Carvalho, and H. He, 2015: Characteristics of mesoscale convective systems over China and its vicinity using geostationary satellite FY2. *J Clim*, **28**, 4890–4907.
- Zhang, W., Z. Huang, F. Jiang, M. F. Stuecker, G. Chen, and F. F. Jin, 2021: Exceptionally Persistent Madden-Julian Oscillation Activity Contributes to the Extreme 2020 East Asian

Summer Monsoon Rainfall. *Geophys Res Lett*, **48**.

Zhang, Y., F. Zhang, C. A. Davis, and J. Sun, 2018: Diurnal evolution and structure of long-lived mesoscale convective vortices along the mei-yu front over the east China plains. *J Atmos Sci*, **75**, 1005–1025.

Zolman, J. L., E. J. Zipser, and K. I. Mohr, 2000: A Comparison of Tropical Mesoscale Convective Systems in El Niño and La Niña. *J Clim*, **13**, 3314–3326.